Materials Science & Engineering C 99 (2019) 1075–1091

Contents lists available at ScienceDirect

Materials Science & Engineering C

journal homepage: www.elsevier.com/locate/msec

Potential of an electrospun composite scaffold of poly (3-hydroxybutyrate)-chitosan/alumina nanowires in bone tissue engineering applications

Elahe Bahremandi Toloue[a], Saeed Karbasi[a,*], Hossein Salehi[b], Mohammad Rafienia[a]

[a] Department of Biomaterials and Tissue Engineering, School of Advance Technology in Medicine, Isfahan University of Medical Sciences, Isfahan, Iran
[b] Department of Anatomical Sciences and Molecular Biology, School of Medicine, Isfahan University of Medical Sciences, Isfahan, Iran

ARTICLE INFO

Keywords:
Bone tissue engineering
Electrospinning
Poly-3-hydroxybutyrate
Chitosan
Alumina nanowires

ABSTRACT

The choice of material types for tissue engineering scaffolds and the design of methods are contributive in yielding the proper result. In this study, 1–5% wt. Alumina nanowires are added to (Polyhydroxybutyrate-Chitosan) PHB-CTS alloy solution, and the scaffolds are prepared by electrospinning method. The fiber diameters, porosity percentages and uniform distribution of Alumina nanowires are assessed by SEM, EDS and TEM. The surface roughness of the fibers is confirmed by FESEM and AFM. The crystallinity of nanofibers is calculated by DSC and verified by FTIR. The tensile strength of the PHB-CTS scaffold increase up to > 10 fold in presence of 3% wt. Alumina. Formation of calcium phosphate sediments only on the surface of Alumina containing scaffolds after 7 and 28 days of immersion in SBF is observed by SEM, and verified by XRD analysis. Proliferation and viability of MG-63 cells and alkaline phosphatase secretion are significantly higher on scaffolds containing Alumina than that of the PHB or PHB-CTS. The appropriate properties of Alumina which affected in cell behavior, hydrophilicity enhancement, bioactivity and mechanical properties make it contribution agent in bone tissue engineering.

1. Introduction

Tissue engineering is a science capable of regenerating the lost or damaged tissue regeneration. An appropriate biological function can be achieved when there exist proper interaction among the scaffold, cells and the environmental factors. Bone tissue engineering, has always been and is one of the interests among researchers due to the great volume of musculoskeletal injuries, rapid growth and its significant potential in physical properties of extracellular matrix [1,2]. Designing and selecting biomaterials consumed in fabricating scaffolds is importance due to their having mimicking extracellular matrix (ECM) [3,4]. These scaffolds should be highly porous, biocompatible and biodegradable, with non-toxic degradation products. During tissue regeneration, these scaffolds should tolerate mechanical stresses. Another requirement for proper scaffolds is to facilitate cell metabolism, proliferation and migration [3,5]. The fibers' structure in the extracellular matrix is easily mimicked by electrospun fibers [6]. Electrospinning is an effective method in producing polymer, ceramic, or composite fibers in a top-down methods. Other methods like gas jet and melt fibrillation and higher precision techniques like self-assembly and nanolithography produces fibers, while the most important advantage of electrospinning method its cost-effectiveness, accessibility and simplicity in mass fiber production [4,6–8]. In the last decade this method, by producing fibers with diameters from nanometers to a few micrometers, has gained fame [4,6,7].

To produce biodegradable scaffolds, both of natural and synthetic polymers, are of concern because of their proper ability in cell adhesion, proliferation, migration, and differentiated function [9,10]. Poly-3-hydroxybutyrate (PHB) as a member of the polyhydroxyalkanoates (PHA) family is a kind of polyester synthesized by microorganisms as the intracellular carbon. Some researchers indicate that PHB is fit for bone tissue engineering due to its favorable physical and mechanical properties with no observed undesirable chronic inflammatory response even one year after implantation periods [11–16]. Moreover, oligomonomers and monomer of PHB, after degradation process are non-toxic with having proper biocompatibility [17]. Studies indicate that *in vitro* and *in vivo* biodegradation of PHB is less than most biodegradable polymers, like PLA and PGA [18]. Brittleness and high degree of crystallinity of PHB is assumed to be the most important limitation in its application in tissue engineering. To improve the low degradation rate, researchers attempt to compose PHB with natural polymers, like chitosan [19], gelatin [20] and cellulose [21]. Chitosan (CTS) is a kind of natural amino polysaccharides which allows cell attachment, cell proliferation and with antibacterial activity is widely consumed for bone

* Corresponding author.
E-mail address: Karbasi@med.mui.ac.ir (S. Karbasi).

https://doi.org/10.1016/j.msec.2019.02.062
Received 30 July 2018; Received in revised form 8 December 2018; Accepted 15 February 2019
Available online 16 February 2019
0928-4931/

Table 1
Materials used in this study.

Row	Material name	Company/County made	Propose
1	Poly-hydroxybutyrate (PHB)	Sigma Aldrich/USA	Scaffolds preparation
2	Chitosan(CTS)	Sigma Aldrich/USA	
3	Alumina nanowires (Al_2O_3)	Sigma Aldrich/USA	
4	Trifluoroacetic acid (TFA)	Merck/Germany	
5	Phosphate-Buffered Saline	Ceram Razi co./Iran	*in vitro* degradation
6	Simulated Body Fluid	Ceram Razi co./Iran	bioactivity assay
7	MG-63 osteosarcoma cell line	Cell Bank of Pasteur Institute/Iran	Cellular evaluation
8	DMEM, Glutamax (low Glucose)	GIBCO/USA	
9	Ethanol(100%)	Arman Sina Chemical/Iran	
10	Fetal bovine serum (FBS)	GIBCO/USA	
11	Penicillin/streptomycin	GIBCO/USA	
12	Trypsin-EDTA (0.25% Trypsin in 0.04 mM EDTA)	GIBCO/USA	
13	3-(4,5-dimethylthiazol-2-yl)-2,5-diphenyltetrazolium bromide (MTT M5655-100 Mg	Sigma Aldrich/USA	
14	Dimethyl sulfoxide (DMSO)	Sigma Aldrich /USA	
15	Glutaraldehyde(25% Aqueous Solution)	Merck/Germany	
16	Triton X-100	Merck/Germany	
17	ALP assay kit	Pars Azmun/Iran	

tissue engineering applications [22–26]. An increase in hydrophilicity of electrospun fibers is observed after adding CTS to PHB solution [19]. The inherent brittleness of fibers reduces after alloying process. The chondrocyte cell adhesion and proliferation are better compared to pure PHB fibers while a reduction is observed in the mechanical properties in the alloying polymer [27,28].

One of the most effective methods for increasing the mechanical properties of polymers is applying ceramics as a reinforcement phase. Studies indicate that higher mechanical properties can be achieved by adding less amounts of nanoscale reinforcement phase compared to conventional polymer composites [7,29]. One-dimensional nanostructures are one of the best choices due to their tendency to be interdiffused and entangled in the polymer host. Studies reveal that the mechanical properties of polymeric nanofibers are enhanced by addition of one-dimensional nanostructures like nanotubes [13,27,30,31], nanowhiskers [32,33], nanorods [34] and nanowires, while nanoparticles can hardly increase these mechanical properties [35]. The electrospinning method has the capacity to align one-dimensional nanostructures with fibers [6,36]. The chosen of proper material as the reinforcement phase in bone tissue engineering scope, must be able to generate bioactivity and enhance mechanical properties. Although some biodegradable or bioactive ceramics can form hydroxyapatite layers, some researchers indicate that the mechanical properties(specially ductility or toughness) are not sufficient increments [37,38]. To enhance the mechanical properties of polymer matrices, the bioceramics like CNT, ZrO_2 and Al_2O_3 are more effective because of their high Young's modulus and tensile strengths [39,40].

Alumina (Al_2O_3; Aluminum oxide) as the first clinical bioceramics is highly consumed in orthopedic [41–43] and dental implants [44–46] due to its chemical inertness, resistance to oxidation, corrosion and biocompatibility [47]. Particle size in Alumina is an important factor in changing its properties. Among the various phases of the Alumina: α, χ, η, δ, κ, θ, γ, ρ the γ-Al_2O_3 nanocrystals are of special importance due to their proper surface properties, like thermal, mechanical and chemical stability, big surface area and porosity [47,48]. Inorganic nanofibers like Alumina, have excellent mechanical properties, similar to their bulk counterparts, with a better perform as reinforcement phases in mechanical properties enhancement of polymer matrices. Alumina nanostructure reveal significant enhancements in mechanical properties of polyvinyl alcohol (PVA) [49], Ultra High Molecular Weight Polyethylene (UHMWPE) [50], Poly(ε-caprolactone)(PCL) [35] and Poly methyl methacrylate (PMMA) [51]. The positive effect of Alumina on PCL electrospun nanofibres reinforced in the ultimate tensile strength are reported by Dong et.al [35]. It could be due to the adhesion between polymer and Alumina. Strong interaction between Alumina nanoparticles and polyesters through polar bonds and hydrogen bonding is reported by Rodriguez-Lorenzo et al. [52]. The biological responses of alumina nanowires in cultured fibroblasts (L929) and macrophages (RAW264) were evaluated by Hashimoto et al. [53]. There is no cytotoxic, genotoxic and nuclear damage observed by using Alumina nanowires.

To the best knowledge of the authors, there exist few studies on the bioactivity properties of Alumina nanostructures. Although Alumina is known as an inert ceramic, its nanostructured type is affected on the osteoblast adhesion compared to conventional structures [54]. The positive effects of nanoporous Alumina are studied on differentiation, growth and proliferation of mesenchymal stem cells (MSCs) [55–57], where high levels of osteoblastic differentiation markers like alkaline phosphatase are observed on nanoporous Alumina substrates. Deposition of calcium-containing mineral and synthesis of alkaline phosphatase on Alumina nanostructured as an evidence of enhanced osteoblast proliferation is assessed by Webster et al. [58].

In this study, Alumina nanowires, as the reinforcement phase in PHB-CTS electrospun nanofibers, are consumed due to their low cost, good compatibility and high modulus. The effect of different percentages amounts of Alumina nanowires on the morphology of fibers, tensile strength and hydrophilicity of the fabricated composite scaffolds are assessed and the results are compared with PHB and PHB-CTS fibers scaffolds. The dimensions of the Alumina nanowires in this study are less than the dimensions of carbon nanotubes, which lead to its easy facilitation at a higher percentage [27,35].

To the best knowledge of the authors here there exist no studies where Alumina nanowires are consumed in PHB electrospun fibers. This is the first attempt made in assessing the bioactivity of Alumina (in the form of nanowires) in polymeric scaffolds. The MG-63 cell viability and attachment is assessed on polymeric fibers with and without Alumina.

2. Materials and methods

2.1. Materials

The materials used in this study are provided in Table 1.

2.2. Preparation of electrospun scaffold

As proposed by Sadeghi et al. study [19], 9% wt. PHB is solved in TFA at 50 °C for 1 h followed by adding TFA, 20% CTS to the solution as the optimum concentration and stirred for 30 min at 60 °C in order to yield PHB-CTS alloy solution. Al_2O_3 nanowires suspension is prepared in TFA, at five different concentrations of (1–5% wt.). This suspension is sonicated by Sonicator (SYCLON, SKL-950W/China) to yield more

Table 2
Constituents of electrospun (in wt%) samples prepared.

Samples	PHB	CTS	Al_2O_3 nanowires
a	9%	0%	0%
b	9%	20%	0%
c	9%	20%	1%
d	9%	20%	2%
e	9%	20%	3%
f	9%	20%	4%
g	9%	20%	5%

uniform dispersion and avoid particle agglomeration. To avoid TFA evaporation, the time for sonication does not exceed 12 s. This suspension is added to the PHB-CTS alloy solution and is mixed with PHB-CTS for 5 min to yield a uniform solution. This prepared electrospinning solution is sucked into a 1 ml syringe, connected to a blunt-end 21G-gauge needle and set in its position. A random fiber structure is formed on the collector covered with aluminum foil. The electrospinning parameters that affect the fiber diameter are the distance between collector and needle, flow rate and voltage. These parameters are optimized based on the Taylor cone formation, absence of droplet formation and SEM images in order to obtain smooth and bead-free fibers. According to this optimization, the distance between the collecting plate and the tip of the needle is adjusted at 25 cm and the injection rate is set at 0.01 ml/min. A high voltage of 22 kV is applied to the tip of the needle of the syringe. The percentage of theses scaffolds are tabulated in Table 2. To remove any residual solvent, these scaffolds are vacuum dried overnight at room temperature to be applied for further experiments.

2.3. Evaluation of scaffolds morphology

2.3.1. SEM

The morphology of the fibers, are assessed by scanning electron microscopy (SEM, SERONTECHNOLOGIES, AIS2100/South Korea) at 1000, 10000 and 25,000 magnifications. The scaffold samples are cut in 1 cm × 1 cm and gold deposited on the scaffolds by applying sputtering (Emitech SC7620 Sputter Coater; Quorum Technologies/UK) before scanning. The mean fiber diameter and their distribution are evaluated through Image J analysis software (Wayne Rasband, National Institute of Health/USA) by choosing 25 fibers from different places of each image at 10000 magnifications. The porosity percentage of the scaffolds is measured through MATLAB (R2016a) software program for the three surface layers.

2.3.2. Field emission scanning electron microscopy (FESEM)

To assess the effect of Alumina nanowires on surface morphology of the electrospun fibers, FESEM (MIRA3TESCAN-XMU/USA and FEI QUANTA 200/Neitherlands) is applied.

2.3.3. Atomic force microscopy (AFM)

To measure the surface roughness on the fibers, AFM of non-contact mode (Dualscope/Rasterscope C26, DME/Denmark) is applied on 1μm^2 and 15μm^2 surface area (n = 3) for PHB-CTS and PHB-CTS/5%Al_2O_3. The root mean square deviation roughness (Sq) is calculated through dme spm software version 2.1.1.2.

2.3.4. Energy dispersive X-ray spectroscopy (EDS)

To obtain the corresponding elemental Mapping, EDS, (EDAX Element Silicon Drift Detector, Apolo) is applied for PHB-CTS/3%Al_2O_3.

2.3.5. Transmission electron microscopy (TEM)

To observe the presence of Al_2O_3 nanowires in the composite scaffold, TEM (EM208S, Philips/the Netherlands) is applied. One layer of electrospun fibers is deposited onto a copper grid attached on aluminum foil on the collector.

2.4. FTIR structural characterization

To evaluate changes in a chemical structure, FTIR& FTIR-ATR (Bruker, Tensor 27/Germany) are applied. FTIR-ATR technique is run over a wavenumber within 600 and 4000 cm^{-1} range at room temperature. FTIR-ATR is run for pure PHB electrospun fibers, CTS film, PHB-CTS electrospun fibers, PHB-CTS/3% Al_2O_3 composite scaffold and FTIR is run for Alumina nanowires.

2.5. Thermal characterization

2.5.1. Thermogravimetric analysis and differential thermogravimetry (TGA, DTG)

To assess the effect of ceramic phase presence in the scaffolds, thermal characterization is applied. Thermal behavior of PHB, PHB-CTS and PHB-CTS/5%Al_2O_3 composite scaffolds is determined by TGA and derivative thermogravimetric (DTG), (Mettler Toledo/USA), according to ASTM-E1131.

2.5.2. Differential scanning calorimetry (DSC)

Melting and crystallization behavior of the scaffolds are studied by differential scanning calorimetry (DSC, NETZSCH STA 449F3/Germany).

For both the TGA and DSC, the sample mass is about 12 mg, sealed in aluminum pans, at a heating rate of 10 °C/min, under a flowing nitrogen atmosphere, the DSC curves is recorded within 50 to 600 °C. The degree of crystallinity (χ_c) is measured through Eq. (1).

$$\chi_c\% = \frac{\Delta H_m/\Phi_{PHB}}{\Delta H_m^0} \times 100\% \quad (1)$$

where, ΔH_m, is the apparent melting enthalpy of PHB matrix in composite specimens, $\Delta H_m{}^0$ is the melting enthalpy of the theoretically 100% crystalline PHB polymer at 146 J/g [59–61], and Φ_{PHB} is the weight fraction of PHB matrix in the composite.

2.6. Analysis of surface hydrophilicity

The surface hydrophilicities of scaffolds, (Table 2) are measured and cultured through contact angle meter (CA-ES10, Fars EOR./Iran) at room temperature. One drop of double deionized water is dropped on three different locations an each scaffold. The contact angles are recorded after 10 s.

2.7. Mechanical characterization

The mechanical properties of scaffolds are run by tensile test, with DIN EN ISO, 05/1995 at room temperature. The fabricated scaffolds are carefully cut into of 30 mm × 5 mm dimensions and the thickness of each sample is measured with a micrometer. The load cell applied here is 20 N, the distance between the two jaws is 20 mm and the extension rate is kept at 1 mm/min. The slope of the stress curve in the linear region of the elastic modulus is calculated as Young modulus.

2.8. Assessing and measuring biodegradability

Nanofiber composite scaffolds are cut into dimensions of 1 cm × 1 cm. Each of them is weighed by a scale of 0.00001 and applied in assessing the *in vitro* degradation. Each scaffold is incubated in 5 ml at 37 °C for 100 days, according to ASTM-F1635. Scaffolds are removed from the solution, rinsed three times with distilled water, dried for 4 h at 37 °C and then weighed. The degradation rate of each scaffolds are calculated through Eq. (2).

$$WeightLoss\% = \frac{W_0 - W_t}{W_0} \times 100\% \quad (2)$$

where, W_0 is the scaffold initial weight in its dry state before being placed in PBS and W_t is the weight of the degraded scaffold at different time intervals. To evaluate pH content change in degradation process, the medium is not refreshed during the degradation period and pH value is recorded by pH Meter (ISTEK, 735P/Korea) once a week for 100 days. The SEM and FTIR analysis are run on PHB-CTS/3% Al_2O_3 composite scaffold after 100-day degradation.

2.9. Bioactivity assessment

PHB, PHB-CTS and PHB-CTS/3%Al_2O_3 composite scaffolds are cut in 1 cm × 1 cm and immersed in 10 ml SBF for 7 and 28 days in an incubation at 37 °C according to ISO 10993-18. The pH solution is measured every week and is fixed within 7.42–7.45. After day 28, the scaffolds are removed from SBF and rinsed three times in distilled water to remove any adsorbed minerals. SEM (ESEM FEI QUANTA 200/ Netherlands) is applied to assess the surface changes in the scaffolds. The semi-quantitative analysis Energy dispersive X-ray analyzer EDS, (EDAX Element Silicon Drift Detector, Apolo) is applied in determining the chemical composition of the mineral surface layer. After 28 days immersion, the X-ray diffraction (XRD) (Bruker, D8ADVANCE/ Germany) analysis is run to assess the mineralization by applying CoKα radiation with a wavelength of 0.17890 nm. In this analysis, step size is 0.05°, and time per step is 2 s, the applied voltage is 40 kV and the angle of diffraction (2θ) is within 10° to 55° range. The X-Pert high score software is applied to recognize the crystallization phases.

2.10. Cell behavior assay

PHB, PHB-CTS and PHB-CTS/3%Al_2O_3 composite scaffolds are cut in circular sheets, at 1 cm radius and sterilized through PBS, ethanol and UV light for 60 min before cell culture and then placed on 24-well plates. The cells are cultured in DMEM medium supplemented with 10% FBS and 1% penicillin-streptomycin. After reaching 80% confluency, the cells are separated by Trypsin-EDTA. These cells are seeded with the density 5×10^3 on each pre-soaked specimen and incubated in a humidified atmosphere containing 5% CO_2 at 37 °C and their medium is refreshed every other day.

2.10.1. Cell viability assay

This assay determines the viable cell count and is based on the mitochondrial reduction in to tetrazolium salt, 3-[4,5-dimethylthiazol-2-yl]-2,5-difenyltetrazolium bromide (MTT), at days 1, 3 and 7, according to ISO-10993-5. In brief, after refreshing the culture medium on the assigned days, 400 µl serum free DMEM and 40 µl MTT solution (5 mg/ml) are added to each well, for 4 h. The yellow MTT dye is turns dark blue formazan by the mitochondrial reductase enzyme in living cells after incubation. The MTT solution is removed, and 200 µl DMSO solution is added to dissolve the formazan crystals. The plate is kept at room temperature for 1 h to assure dissolution of formazan. The dissolved formazan solution is added to 96-well plate (100 µl per well). The absorbance values of each solution are measured through a microplate reader (680, Bio-Rad, Hercules, CA/USA) and the optical density (OD) is measured at 570 nm wavelength.

2.10.2. Cell morphology studies

The morphology and adhesion of MG-63 cells on the PHB, PHB-CTS and PHB-CTS/3% Al_2O_3 composite scaffolds are assessed on day 1 and 7 after being cultured by SEM. The scaffolds are rinsed three times with PBS and next are immersed in glutaraldehyde (3%) as a fixation solution and then placed at 4 °C for 1 h. After removing glutaraldehyde, scaffolds are immersed in 50, 70, 90, and 100% ethanol for 30 min at a time, at 4 °C to become dehydrated. The scaffolds are dried and after being coated by AU-Pd (Gold-Palladium) and their images are taken by SEM (ZEISS/Germany).

2.10.3. Alkaline phosphatase activity assay

Alkaline phosphatase (ALP) is a biochemical marker applied in differentiating and mineralizing to evaluate of scaffolds for MG-63 cell [4]. Alkaline phosphatase is an enzyme that causes of separation phosphate from *p*-nitrophenyl phosphate, and converts it into p-Nitrophenol (PNP). Light absorbance of the yellow PNP, is measured as a guideline to ALP activity. DMEM is removed on first, second and third weeks from scaffolds and rinsed twice with PBS. The cells are centrifuged for 10 min at speed of 2000 for 10 min after being transferred to the eppendorf, then the PBS are removed and 20 µl of Triton X-100 is added to the eppendorf and placed in the refrigerator at −20 °C for 30 min. One milliliter of the alkaline phosphatase solution, prepared according to manufactures guidelines, is added into the eppendorf. Then, 100 µl of this Eppendorf is poured in the 96-well plate and read by microplate reader (680, Bio-Rad, Hercules, CA/USA) at 405 wavelengths.

2.11. Statistical analysis

All experiments are run in triplicate. The results are expressed as the means ± standard error (SE). A value of $p < 0.05$ is considered to be statistically significant. The one way ANOVA analysis is applied to compare the samples.

3. Results and discussion

3.1. Evaluation of scaffold morphology

3.1.1. Scanning electron microscopy (SEM)

Electrospinning is a powerful and appropriate technique for production of 3-D scaffolds applied in tissue engineering based on bending instability, which both of the fiber diameters and their distribution are important [62]. SEM images are show in Fig. 1, where the fully porous, uniform and bead-free structure of the prepared scaffolds can be observed.

The histogram of the composite fibers is given to determine the fiber diameters and their distribution. The fiber diameters and their average porosity percentage of these samples are tabulated in Table 3.

Adding CTS to PHB can have two contradictory effects on the fiber diameter. a) Decrease in fiber diameters, because CTS has positive charge, thus, the solution tendency to be sprayed from the syringe decrease. The same trend is observed in [28,63]. b) Some new intermolecular hydrogen bonds are formed between carbonyl groups of PHB and amino groups in CTS. These bonds formation can enhance surface tension and cause an increase in fiber diameter. This increase is observed after CTS is added to PHB [64] and added to PLA [65].

In this study it is observed that the fiber diameters significantly increase from 321 nm for PHB pure electrospinning fibers to 426 nm for PHB-CTS alloy polymer ($p < 0.05$). After adding Alumina it is observed that the fiber diameters become significantly larger, from 426 nm to 645 nm ($p < 0.05$). There exist studies where in some ceramic-polymer solutions like $CaCO_3$ and HA in PCL [66] and Aluminum Oxide whiskers in PCL [35], the average of fiber diameters become larger when the concentration of these ceramics increase in the polymer solutions. This fact may be due to non-electrical conductivity inherent in these ceramics. An increase in the Alumina in high concentration, sometimes leads to observable agglomerations in SEM images especially at 5% wt. Alumina (Fig. 1(g)). High agglomeration in polymer solution cause a reduction in tensile force at the jet point which increases the diameter of the fibers and the distribution of the fibers in an asymmetric manner [28]. The presence of thick and thin fibers together in PHB-CTS/5%Al_2O_3 image and its high standard error in the fiber diameters in Table 3 are resulted from the high

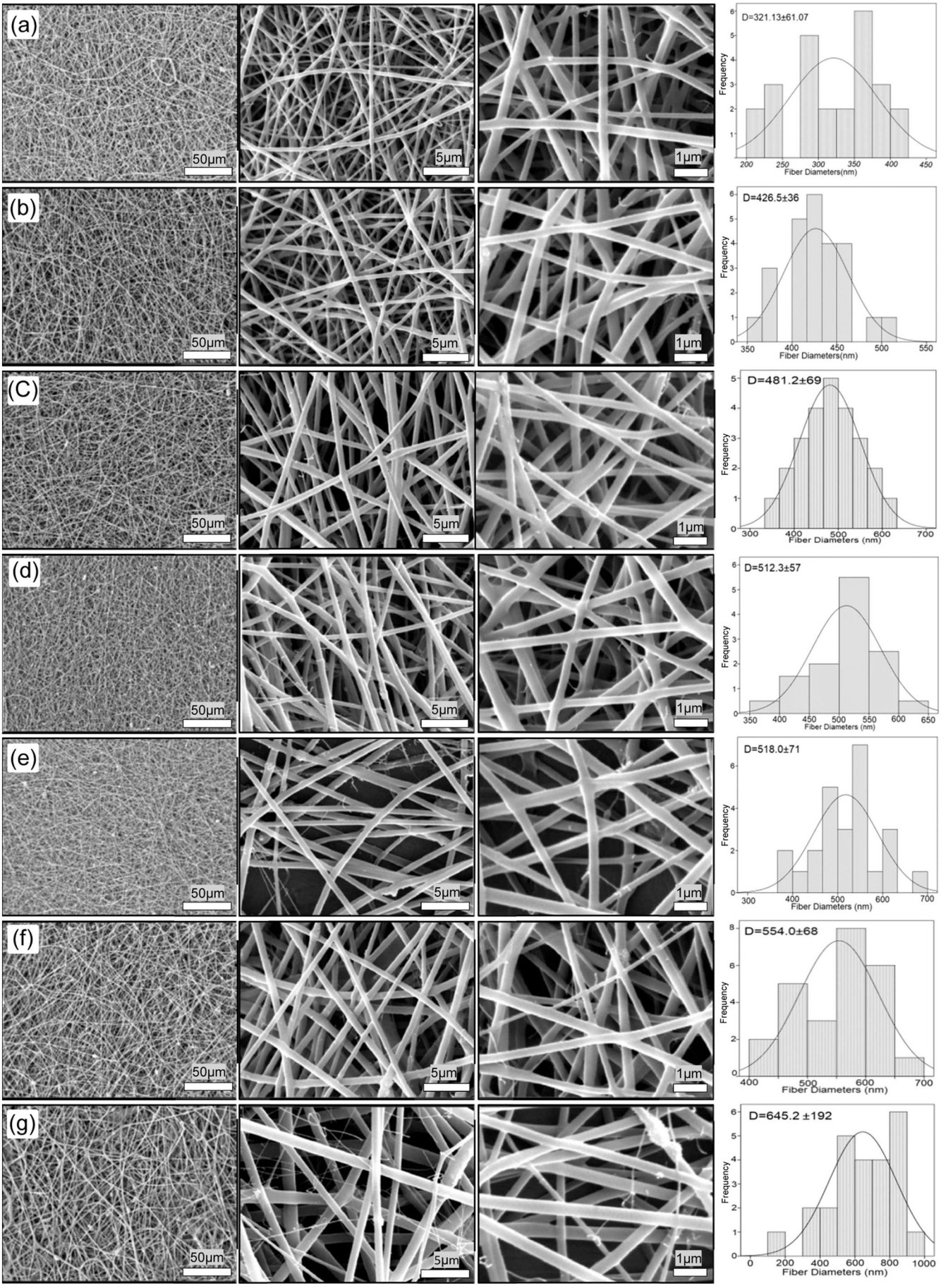

(caption on next page)

Fig. 1. SEM images at 1000, 10000 and 25,000 magnifications and histograms illustrating the diameter distribution of (a) PHB, (b) PHB-CTS, (c) PHB-CTS/1%Al_2O_3, (d) PHB-CTS/2%Al_2O_3, (e) PHB-CTS/3%Al_2O_3, (f) PHB-CTS/4%Al_2O_3, (g) PHB-CTS/5%Al_2O_3.

Table 3
The average fiber diameters of the scaffolds and the porosity percentage are assessed through Image J and MATLAB softwares, (a) PHB, (b) PHB-CTS, (c) PHB-CTS/1%Al_2O_3, (d) PHB-CTS/2%Al_2O_3, (e) PHB-CTS/3%Al_2O_3, (f) PHB-CTS/4%Al_2O_3, (g) PHB-CTS/5%Al_2O_3.

Samples	Average fiber diameters(nm)	Porosity percentage		
		First layer	Second layer	Third layer
(a)	321.1 ± 61	81.70	51.71	20.14
(b)	426.5 ± 36	81.51	46.61	22.09
(c)	481.2 ± 69	82.92	46.04	20.50
(d)	512.3 ± 57	81.89	47.45	21.75
(e)	518.0 ± 71	81.38	48.11	25.95
(f)	554.0 ± 68	80.11	50.93	21.64
(g)	645.2 ± 192	79.75	47.53	24.00

agglomeration.

The morphology of the fibers like diameter, pore size and porosity of scaffolds influence cell behavior [67]. The volume of porosity is an important issue for oxygen and moisture penetration and channeling nutrients into the interior and the waste exit from the cells. In this study the porosity percentages of the scaffolds are illustrated through MATLAB for three layers of each sample similar to other researchers [68,69]. The results of all specimens are tabulated in Table 3; where as observed in the first layer, for all scaffolds (except 5% Alumina) porosity is above 80%, which is appropriate in tissue engineering. In 5% Alumina, increasing fiber diameter and presence of agglomeration can cause a reduction in porosity [28]. For second and third layers the porosities are about 40 and 20%, respectively, demonstrating interconnectivity in pores with a positive effect on cell growth [68]. The results indicate that by adding Alumina and CTS in PHB, the proper fiber diameters and porosity percentages are considered as the initial necessary condition for electrospun scaffolds in tissue engineering.

3.1.2. Field emission scanning electron microscopy (FESEM)

For more accurate details the surface morphology of fibers is assessed by FESEM. The images of PHB-CTS and PHB-CTS/5%Al_2O_3 are shown in Fig. 2. As observed, the fibers without Alumina are smooth and the ones with Al_2O_3 are wrinkled. This wrinkling causes increase in surface roughness, which could better cell adhesion and cell proliferation. Formation of wrinkles become enhanced after adding Al_2O_3 whisker to PCL electrospun fibers [35], who reported that an increase in wrinkles can increase surface roughness and could mimic the natural extracellular matrix (ECM) more closely.

3.1.3. Atomic force microscopy (AFM)

Cell adhesion as an important key in tissue engineering technology is mostly influenced by surface roughness [70]. PHB-CTS and PHB-CTS/5% Al_2O_3 composite scaffold are analyzed by AFM to assess the effect of Alumina presence in fibers. The results are shown in Fig. 3, where that topography of PHB-CTS/5% Al_2O_3 composite scaffold reveal that more tops and valleys are compared with that of PHB-CTS. The average roughness (Sq) of PHB-CTS is 346.2 ± 23 nm, while significantly increased to 492.6 ± 67 nm after adding Alumina, ($p < 0.05$). The surface roughness for one of the fibers is evaluated as well; 28.3 ± 12 nm and 79.5 ± 23 nm are given for PHB-CTS and PHB-CTS/5%Al_2O_3, respectively. Previous studies reveal that osteoblasts, fibroblasts, smooth muscle cells, chondrocytes and endothelial cells respond better to surface roughness in nanometer compared to smooth surface [71,72]. Chen et al. assumed the positive influence of surface roughness of electrospun scaffolds on skeletal differentiation of human mesenchymal stromal cells (hMSCs) [4].

3.1.4. Energy dispersive X-ray spectroscopy (EDS)

Fig. 4 is showing the map of EDS. The white dots which related to Al, demonstrate the uniform distribution of Alumina nanowires in PHB-CTS/3%Al_2O_3. This result is the evidence of well-distributed Alumina nanowires in PHB-CTS/3%Al_2O_3 composite scaffolds. The appropriate mechanical properties and biocompatibility of the scaffolds can be due to uniform distribution of reinforcement in the host matrix, making the evaluation of nanowires location essential [73–75].

3.1.5. Transmission electron microscopy

The TEM image of electrospun fiber PHB-CTS/5%Al_2O_3 composite scaffold is shown in Fig. 5; where as observed the Alumina nanowires are aligned in the fibers. This alignment is due to the ability of single-dimensional nanostructures in the electrospinning process [6,36]. Although the Alumina nanowires applied here are of 200–400 nm in length and 4–6 nm in diameters, they appear bigger. This phenomenon can be a sing of interfacial interactions as mentioned by Ciprari et al. [76].

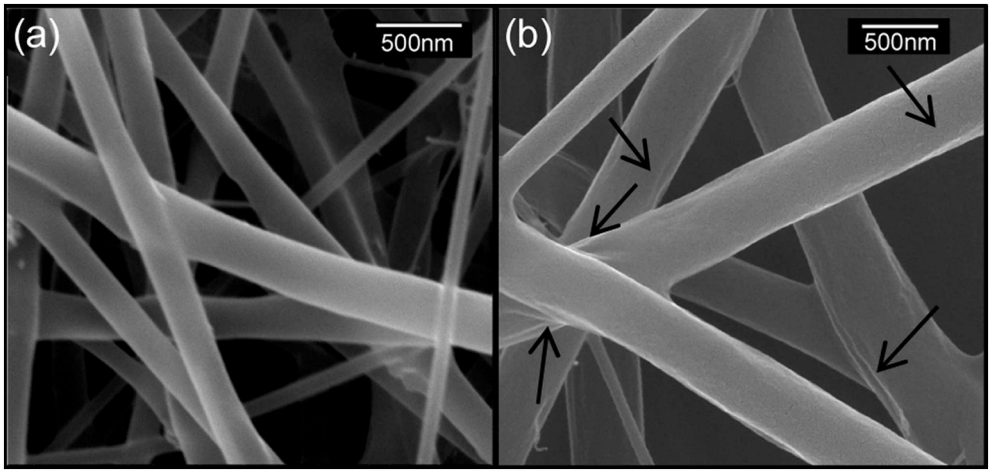

Fig. 2. FESEM images for (a) PHB-CTS and (b) PHB-CTS/5%Al2O3 composite scaffold.

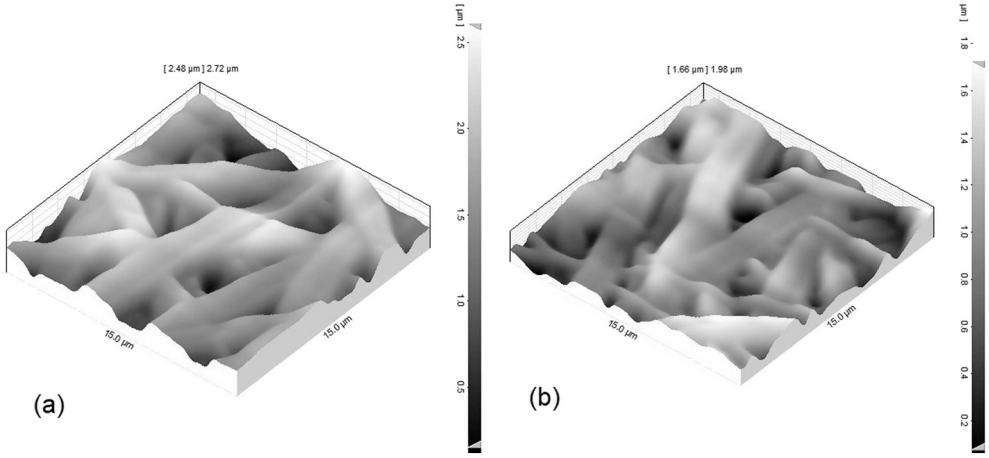

Fig. 3. The 3D images of AFM for (a) PHB-CTS and (b) PHB-CTS/5%Al_2O_3 composite scaffold.

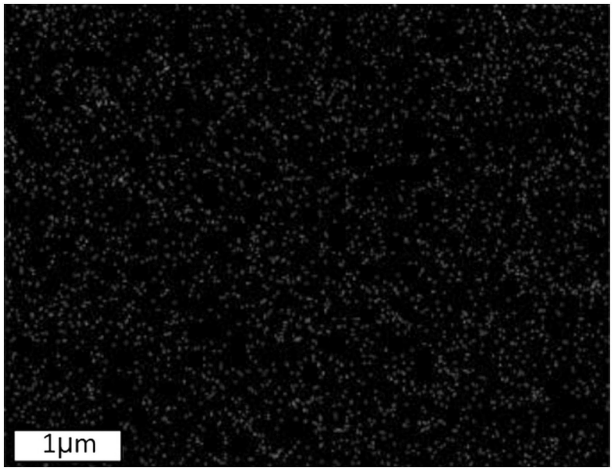

Fig. 4. Presence of Aluminum in nanofiber electrospun in PHB-CTS/3%Al_2O_3 composite scaffold.

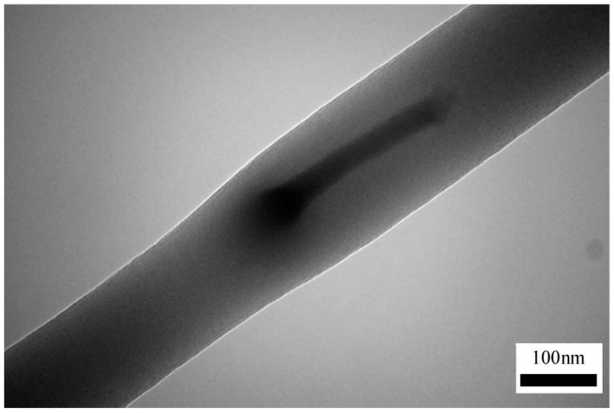

Fig. 5. Presence of Alumina nanowires in PHB-CTS/5%Al_2O_3 electrospun fibers.

3.2. Fourier transform infrared spectrometry

FTIR and FTIR-ATR tests are run to characterize the functional groups of polymers and Alumina addressed in this study. FTIR absorption bands are applied to evaluate both the crystallinity in polymers and the evidences on miscibility of the blend polymers [77–79]. The results of these tests are shown in Fig. 6 and tabulated in Table 4.

The spectrum of the pure PHB scaffold is shown in Fig. 6(a). The characteristic of PHB band at 1720 cm^{-1} is related to stretching absorption of carbonyl group, (υC═O) as the crystalline phase of PHB [69,79,80]. The 980 cm^{-1} correspond to C—C stretching [69,79,81], 1227 cm^{-1} for C—O—C stretching [69,79,82] and 1276 cm^{-1} for symmetric C—O—C stretching [21,69,79–83] as crystalline phase of the PHB. The absorption at the peak 1184 cm^{-1} is attributed to asymmetric C—O—C stretching groups which arise from the amorphous phase of PHB [69,79,80,83]. Carboxyl group (υC—H) appear at 2794–3041 cm^{-1} range [21] and 3433 cm^{-1} refers to hydroxyl end groups (υO—H) [21]. The spectrum of CTS film (prepared by solving in TFA) is shown in Fig. 6(b). The peaks at 3540 cm^{-1} are attributed to the overlapped O—H hydroxyl groups and 3360 cm^{-1} N—H stretching vibrations [84,85].

In higher wavenumbers there exists a broad asymmetric band at around 2948 and 2866 cm^{-1} [84], attributed to the C—H stretching modes. The peak at 1650 $cm^{-1}$and 1597 cm^{-1} is related to amide I,II, respectively [84,86]. The peak at 1076 cm^{-1} is attributed to characteristic polysaccharide bands. The spectrum of PHB-CTS fibers scaffold is shown in Fig. 6(c), where as observed there exist small shoulder at 1670 cm^{-1} near the peak at 1724 cm^{-1}. For CTS amid I in 1650 cm^{-1} small shift is observed toward 1670 cm^{-1} and stretching absorption of carbonyl group of PHB shifts from 1720 to 1724 cm^{-1}, related to miscibility and interaction between PHB and CTS [86]. Other researchers have observed a shift toward higher wavenumber for PHB carbonyl groups' after adding CTS, and have explained that by disturbances in the crystalline portion [69]. It is notable that intensity of carboxylic group peaks (2794–3041 cm^{-1}) is reduced after adding CTS to PHB. This is due to formation of intramolecular hydrogen bonds between the carbonyl groups in PHB and amine functional groups in CTS. The FTIR spectrum of Alumina nanowires are shown in Fig. 6(d), where there exist broad bands around 660 and 867 cm^{-1} attributed to Al—O—Al and Al—O stretching mode, respectively [50,87–90]. The spectrum of PHB-CTS/3% Al_2O_3 composite scaffold is shown in Fig. 6(e). The total effect of Alumina nanowires after adding in to PHB-CTS alloy relatively decreases the intensity of peaks in the 500–1000 cm^{-1} region and increases the intensity after 1000 cm^{-1}. Successful adding of Alumina nanowires in this scaffold are approved by observing two closed peaks in this spectrum at 806 and 820 cm^{-1}, where the first is related to Alumina nanowires and the second is attributed to PHB-CTS. In PHB-CTS/3%Al_2O_3composite scaffold spectrum, the intensity of carboxylic group peaks (2794–3041 cm^{-1}) is reduced after adding Alumina. This is a sign of polar coupling and hydrogen bonding, which could cause proper adhesion between polymers and Alumina [91,92].

To study the changes in polymers' crystallinity, the FTIR absorption spectrum is applied as well. The crystallization of pure PHB is determined by calculating the ratio between the bands at 1184 cm^{-1} and

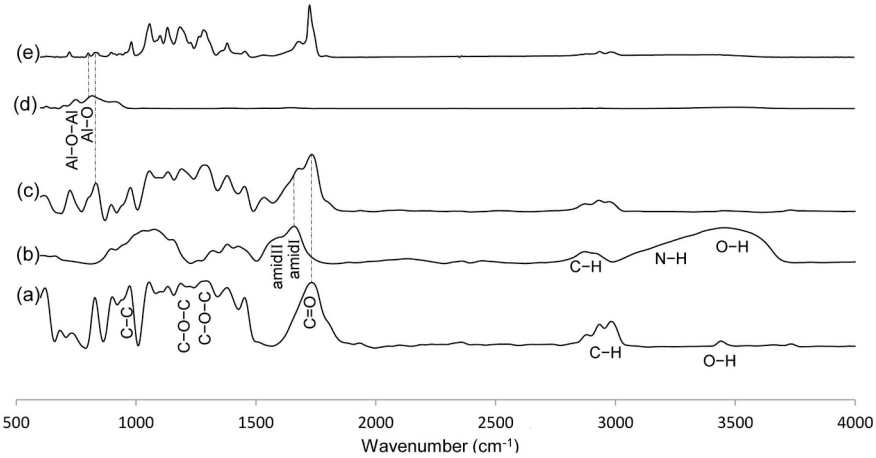

Fig. 6. The FTIR-ATR spectrum of (a) PHB fibers, (b) CTS film, (c) PHB-CTS fibers, (d) FTIR spectrum of Alumina nanowires, (e) PHB-CTS/3%Al_2O_3 composite scaffold.

Table 4
Absorption indexes (AI) calculated through the ratio A_{1228}/A_{1453}.

Specimen	A_{1228}	A_{1453}	$AI = \frac{A_{1228}}{A_{1453}}$
PHB	18.00	14.73	1.22
PHB-CTS	12.76	9.89	1.39
PHB-CTS/3%Al_2O_3	4.20	1.96	2.48

1382 cm^{-1} intensities by [93], while the ratio between the bands at 1228 cm^{-1} and 1453 cm^{-1}intensities are assumed as absorbtion index (AI) by [77,94,95]. Here, this ratio is calculated and tabulated in Table 4.

Although the decrement of crystallinity after adding CTS to PHB is not observed in Table 4, some researchers have found a decrease in crystallinity after adding CTS to PHB [86,96–98]. Formation of hydrogen bonding after adding CTS to PHB act as bridges between two polymers; consequently, facilitating miscibility of the polymers in the blend fibers and prevent crystallinity. Crystallinity of pure PHB fibers are reduced from 67.5% to 37.7% after adding CTS in ratio(50:50) [69].This reduction in crystallinity is observed after adding CTS to other polyesters like PCL [85]. After adding Alumina, as observed, in Fig. 6(e), the peak at 1724, which is related to crystalline phase, becomes sharper. Furthermore in Table 4, the absorption index (AI) becomes greater. The Alumina nanowires act as nucleating agents, leading to an increase in crystallinity degree.The same trend is reported after adding titanium dioxide nanoparticles to PCL solution [99] and adding Zinc oxide nanopowder to Poly(3-hydroxybutyrate-*co*-3-hydroxyvalerate) [100,101]. This increase in crystallization could affect the mechanical properties [102] and degradation rate [103]; moreover it can affect fiber diameters.

3.3. Thermal characterization analysis (TGA, DTG)

The thermal behavior of the PHB, PHB-CTS and PHB-CTS/5% Al_2O_3 composite fibers are analyzed through TGA and DTG, Fig. 7. The initial decomposition temperature (T_i) and the final decomposition temperature (T_f) are extracted from TGA and the temperature at which the maximum mass decomposition occurs (T_d; as a criterion of thermal stability) is extracted from DTG and the results are tabulated in Table 5. All 3 specimens expose single stage mass in TGA. For PHB fibrous scaffolds, before T_i: 235 °C, approximate 3% weight loss is observed due to volatilizing of low-molecular-weight materials like water. Here, the T_d for PHB fibers occurs in around 260 °C due to degradation of PHB chains, and the same value is reported by [77,81]. After T_f (277 °C) no significant weight loss is observed. For PHB-CTS, T_i decreases to 217 °C compared to that of pure PHB. This decrease could be the result from proper miscibility and compatibility between the two polymers, which is reported for PVA-PHB by Asran et al. [69]. The thermal stability of PHB-CTS blending alloy (T_d: 268 °C)is slightly higher than pure PHB [69,104].

After adding Alumina, T_i begins at the same temperature where the PHB-CTS scaffold begins. The degradation rate of the scaffolds with Alumina is slower than the others. This slow degradation rate is due to incorporation of Alumina into the scaffolds [87]. After Alumina is added the T_d increases from 268 to 271 °C due to the ceramic content, as expected. These obtained results indicate that the fibers reinforced with ceramic, decompose at a higher temperature with a slower gradient, which is reported by [101,105].

3.3.1. Differential scanning calorimetry (DSC)

When assessing DSC, in addition to obtaining information on the thermal behavior of the scaffolds, it is possible to estimate the alloying effect of and reinforcement addition on the crystallization process. Here electrospinning process could improve crystallization degree because during the electrospinning, polymer molecules have the tendency to be oriented in the fibers direction [59]. The DSC curve of PHB, PHB-CTS and PHB-CTS/5%Al_2O_3 composite scaffold is shown in Fig. 8, where for all 3 specimens, there exist two endothermic peaks attributed to the melting temperature (Tm_1, Tm_2). Tm_1 corresponds to the melting of the as-formed PHB crystals in electrospun fibers, and Tm_2 is attributed to the recrystallized PHB crystals formed during DSC heating [69,106,107]. The melting point of these specimens and the crystallization degree are obtained from the first endothermic peaks of DSC and calculated, respectively, Table 5. For PHB fibers Tm_1 is 179 °C and the enthalpy is 67(J/g). Both of melting temperature and enthalpy decrease after alloying [107]. The CTS as an amorphous polymer slows the crystallization rate of PHB, consequently, the melting point of PHB-CTS decrease [69,107]. One of the reasons for the lowering of melting temperature is the proper miscibility of the two polymers. A decrease in lamellar thickness in PHB crystallites after adding CTS, because of the formation of new Hydrogen bonding can be another reason [86]. The same effect is observed after adding CTS to PLA [106] and adding CTS to PHB [69]. The crystallization degrees for PHB is calculated 45.89%, while after adding CTS, it decreases down to 42.49%. Alumina nanowires act as nucleating agents and increase the crystallinity up to 50.17%.

3.4. Analysis of surface hydrophilicity

Hydrophilic surfaces usually present proper spreading, proliferation and differentiation with an important effect on the field of tissue

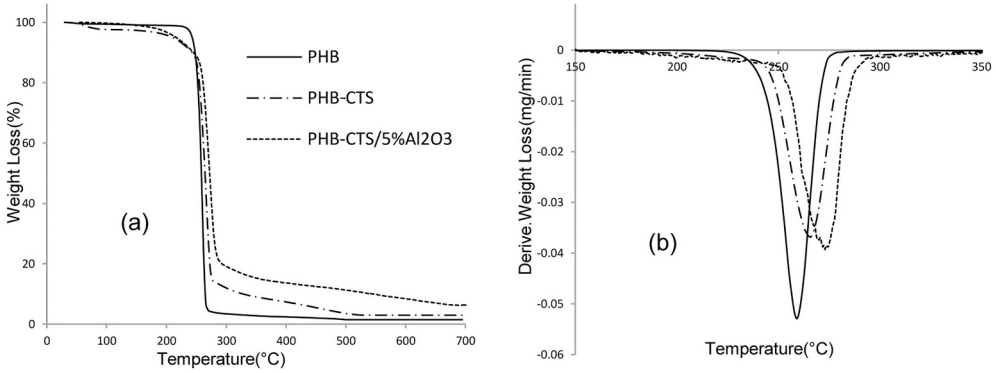

Fig. 7. (a) TGA and (b) DTG for PHB, PHB-CTS and PHB-CTS/5%Al_2O_3 composite scaffolds.

Table 5
T_i, T_d, T_f, Tm_1, ΔH_{m1} and χ% for PHB, PHB-CTS and PHB-CTS/5%Al_2O_3 composite scaffolds.

Samples	T_i (°C)	T_d (°C)	T_f (°C)	Melting point; Tm_1(°C)	ΔH_{m1} (J/g)	Degree of crystallization (χ%)
PHB	235	260	277	179	67.0	45.89%
PHB-CTS	217	268	290	166	51.7	42.49%
PHB-CTS/5%Al_2O_3	217	271	310	157	57.6	50.17%

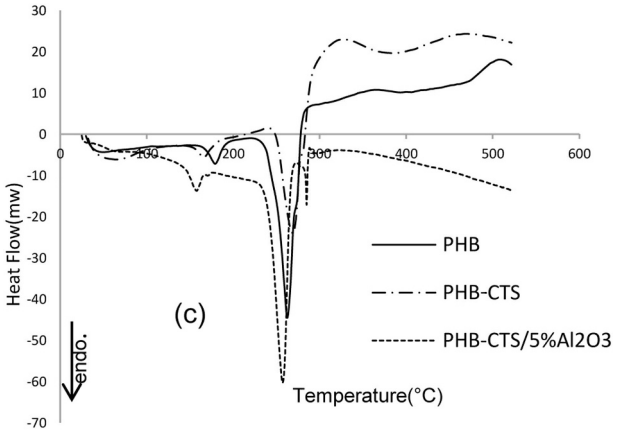

Fig. 8. DSC curves of PHB, PHB-CTS and PHB-CTS/5%Al_2O_3 composite scaffolds.

engineering [80]. Water contact angle (WCA) is a common method adopted testing hydrophilicity of fibers scaffolds [63]. The results for all specimens in Table 2 for this measurement are tabulated in Table 6. The PHB as a polymer with low hydrophilicity, has a major contact angle among the other specimens, as expected. The value is 80.5 ± 2.0°, which is reported by [27,79], while after adding CTS as a natural polymer, it decreases down to 54.3 ± 0.9° at contact angle ($p < 0.05$). After adding Al_2O_3, a significant decrease is observed; from 45.6 ± 1.1° to 30.3 ± 0.7° for 4% Al_2O_3 ($p < 0.05$), while at 5% Al_2O_3 this angle slightly increases to 32.1 ± 1.0°. Contact angle does not depend only on the material composition but depends on surface features like roughness [21,63]. Adding Alumina has two controversial effects on WCA: A, i) its hydrophilic nature and ii) formation of hydrogen bounding in the composite scaffold [108] which decrease in WCA, observed in 1–4% wt. Alumina, while adding higher amounts of Alumina, especially 5%: B, i) increasing the crystallinity of the fibers (FTIR and DSC results), ii) increasing in the fiber diameters and disrupt their uniform distribution (SEM results) and iii) increasing in surface roughness of the fiber (FESEM and AFM results) leads to the trapped air bubbles in the fibers and cause a slight increase in WCA, which is observed in similar researches [21,104].

3.5. Mechanical analysis

Scaffolds designed for bone tissue engineering, in addition to requiring proper degradation, cell growth and biocompatibility must have proper mechanical properties in bearing load. The tensile strength and modulus can be assessed for mechanical properties of electrospun fibers. In order to regenerate a new tissue through composite scaffolds, the volume of reinforcement is optimized based on the mechanical analysis. The results of the stress-strain curve in PHB, PHB-CTS and PHB-CTS/(1–5%) Al_2O_3 composite scaffolds are tabulated in Table 7. Although PHB has proper mechanical properties compared to other polymers, it is not sufficient for it to be applied on its own in skeletal engineering scaffolds due to its low hydrophilic nature and inherent brittleness. Presence of CTS in PHB next to enhanced hydrophilicity, reduce the tensile strength from 2.81 ± 0.15 MPa to 0.89 ± 0.26 MPa and the modulus from 126.3 ± 22.2 to 44.6 ± 0.2 MPa in a significant manner ($p < 0.05$). This decrease is reported by other researchers [27] and it might due to a decrease in crystallinity. Alumina nanowires as reinforcement phases can improve the mechanical properties. The obtained results indicate that an increase in nanowires volume in the scaffold at 3% wt increase the tensile strength became > 10 fold (11.18 ± 1.24 MPa) in relation to PHB-CTS. Placing nanowires along the fibers in uniform distribution are contributed to external forces tolerance. The strong interfacial adhesion between the phases, formed by the hydrogen bonding should not be ignored. There exist an

Table 6
Water contact angle for (a)PHB, (b)PHB-CTS, (c)PHB-CTS/1%Al_2O_3, (d)PHB-CTS/2%Al_2O_3, (e)PHB-CTS/3%Al_2O_3, (f)PHB-CTS/4%Al_2O_3 and (g)PHB-CTS/5%Al_2O_3.

Samples	(a)	(b)	(c)	(d)	(e)	(f)	(g)
WCA	80.5 ± 2.0	54.3 ± 0.9	45.6 ± 1.1	45.3 ± 1.1	31.1 ± 0.7	30.3 ± 0.7	32.1 ± 1.0

Table 7
Mechanical properties (tensile strength and moduluse) of electrospun samples ($n = 3$) for (a) PHB, (b) PHB-CTS, (c) PHB-CTS/1%Al2O3, (d) PHB-CTS/2%Al2O3, (e) PHB-CTS/3%Al2O3, (f) PHB-CTS/4%Al2O3, (g) PHB-CTS/5%Al2O3, (Statistical difference with $p < 0.05$).

Scaffolds	Tensile strength (MPa)	E-Modulus (MPa)
(a)	2.81 ± 0.15	126.3 ± 22.2
(b)	0.89 ± 0.26	44.6 ± 0.2
(c)	1.80 ± 0.15	154.1 ± 39.0
(d)	6.38 ± 0.77	176.8 ± 31.1
(e)	11.18 ± 1.24	539.0 ± 54.9
(f)	4.28 ± 0.50	120.5 ± 92.6
(g)	1.79 ± 0.28	58.6 ± 8.9

appropriate interconnection between Alumina and polymers composites caused by hydrogen bonding at the presence of carboxylic ester groups and Alumina [90,92]. The strong interface between Alumina nanoparticles and PVA is to increase the ultimate tensile stress and modulus in electrospun fibers [109]. Although some authors have emphasized on the contributive aspect of crystallinity on mechanical properties effects of PHB electrospun fibers [108], it is assumed that this slight increase in fiber crystallinity on its, own is not responsible for this abrupt effect on mechanical properties [110]. According to Arinstein et al. an abrupt increase in modulus in polymeric fibers may be attributed to more ordered structure of the fibers [110]. This increase in the ordered structure, in addition to crystallization degree, includes some parameters like the orientation of crystallites in the fiber axis and the orientation of the macromolecule in the amorphous segments [110]. This scope in this field needs more research. One of the most abrupt effects on Young modulus is observed when the diameters of the fibers are around 500 nm [111,112]. Adding higher amounts of Alumina nanowires, especially at 5%, increase fiber diameters, disturbs their uniform distribution and causes agglomeration in the nanowires. Presence of these agglomerates, not only act as stress concentration points, but reduce the mobility of the polymeric chain [28], thus a reduction in crystallinity. The above mentioned phenomena at 5% Alumina can reduce Stress to 1.79 ± 0.28 MPa in significant manner ($p < 0.05$). According to the mechanical analysis and the SEM results, the PHB-CTS/3% Al_2O_3 composite scaffold is selected for the following analysis with respect to PHB and PHB-CTS.

3.6. In vitro degradation

Because the regeneration of new tissue on scaffolds is essential in predicting PHB-base composite scaffold behavior, *in vitro* evaluation of the composite biodegradation is essential. The mechanism of *in vitro* degradability of PHB, PHB-CTS and PHB-CTS/3% Al_2O_3 composite scaffold are evaluated by immersing them in a PBS solution for 100 days.

3.6.1. Morphology of the fibers

The surface morphology of PHB-CTS/3% Al_2O_3 composite scaffold changes after 100 days *in vitro* degradations, Fig. 9. Studies reveal that degradation rate varies in different polymers. Any change in surface morphology in polymers is often of two types: surface melting and fiber breaking. Melting occurs in amorphous segments to reduce surface tension, while breaking of fibers in crystalline segments is due to their rigidity and immobilization [15,113].

3.6.2. Weight loss evaluation

The PHB as a polymer with low hydrophilicity, is subject to surface erosion [114,115], while CTS is subject to bulk degradation due to its hydrophilic nature [116]. The weight loss percentages are shown in Fig. 10. The three scaffolds of concern here reveal an initial slow weight loss, which is appropriate for tissue engineering applications. The PBS can penetrate into polymer network and increases degradation rate through hydrolytic degradation. Although electrospun fibers have high surface-to-volume ratio, and its high porosity is an advantage to increase the degradation rate, while PHB fibers have long degradation time [21]. Hydrophilic nature of CTS can be one of the important factors for an increase in degradation rate for PHB-CTS alloy, while a decrease in the water contact angle can be another important factor (Table 6). The amorphous tendency of the scaffold after adding CTS should not be ignored. The same effect is observed when adding cellulose acetate in PHB solution [21].

Here, it is observed that degradation rate follows the following trend: PHB-CTS > PHB-CTS/3% Al_2O_3 > PHB scaffold. This phenomenon can be explained by paradoxical performance of Alumina, that is as an inert bioceramic, it does not solve in PBS and with holds the scaffolds weight, while due to its hydrophilic nature, increases the degradation rate as to of weight loss.

3.6.3. Changes in pH

The incubation medium of pH volumes for PHB, PHB-CTS and PHB-CTS/3% Al_2O_3 composite scaffolds are shown in Fig. 11, where the initial pH of PBS is 7.4. In general pH tends to decrease during degradation time and this may be due to production of hydroxybutyric acid, which is produced through PHB degradation [3] or due to presence of carboxyl and hydroxyl groups in polymer structure [28]. This reduction in pH for PHB-CTS is higher than other scaffolds and approaches 6.8 at day 100. This observed reduction is similar to that of the weight loss reduction trend: PHB-CTS > PHB-CTS/3%Al_2O_3 > PHB scaffolds. It should be noted that in degradation process, long chains are converted into short chains. These monomers as catalyzers accelerate degradation process and cause a decrease in pH [28].

3.6.4. FTIR assessment

The FTIR-ATR spectrums for PHB-CTS/3% Al_2O_3 composite scaffolds as spun and its degradation on day 100, within 600–2000 cm^{-1} Wavenumber rang is shown in Fig. 12. Amorphous structure

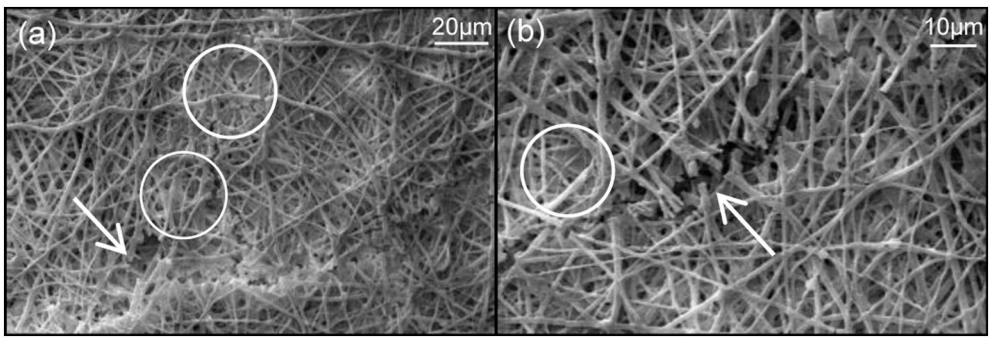

Fig. 9. SEM images for *in vitro* degradation after 100 days, 1500 and 2500×. The arrows show fiber breakage and circles show surface melting.

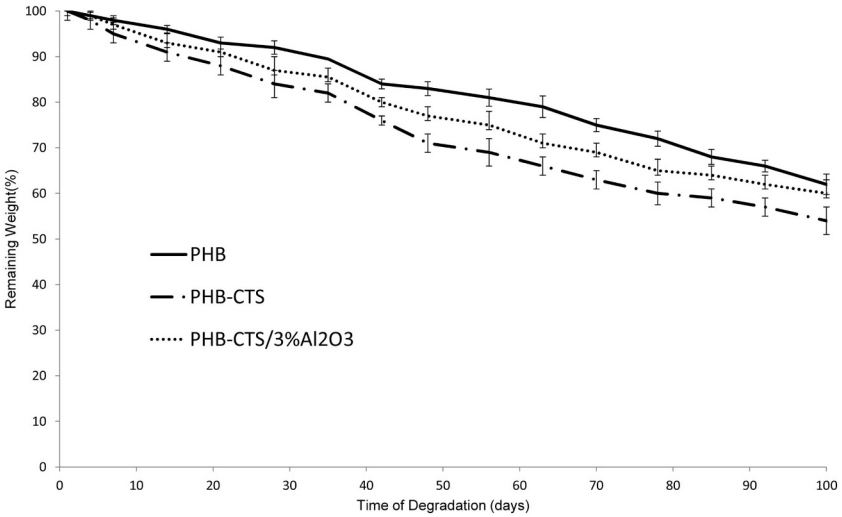

Fig. 10. Weight loss percentages for PHB, PHB-CTS and PHB-CTS/3%Al_2O_3 nanowires electrospune fibers within 100 days immersion in PBS (Statistical difference with $*p < 0.05$).

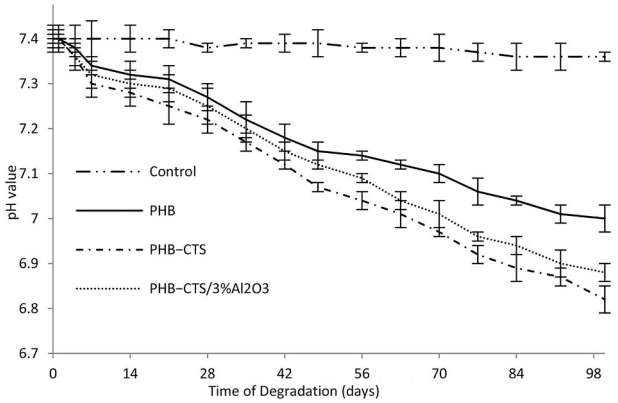

Fig. 11. The pH of the incubation medium for PHB, PHB-CTS and PHB-CTS/3% Al_2O_3 nanowires scaffolds within 100 days immersion in PBS.

degradation occurs twenty times faster than crystalline segments [115]. This can be due to the disordered nature of molecular chains in amorphous segments, which leading to less density. As observed, the intensity increases at peaks 980, 1227, 1284 and 1720 cm^{-1} wavenumber which is attributed to crystalline phase of composite electrospun fibers, while no change is observed at 1184 cm^{-1}, and the later corresponds with the amorphous phase of the composite. A decrease is observed in intensity at 1670 cm^{-1} (amide I, CTS) after degradation. Hydrolyzes of CTS bonds might be a reason for this reduction.

Table 8
Absorption indexes (AI) calculated through the ratio A_{1228}/A_{1453}, for PHB-CTS/3%Al_2O_3 as spun and at 100 day degradation.

Specimen	A_{1228}	A_{1453}	$AI = \frac{A_{1228}}{A_{1453}}$
PHB-CTS/3%Al_2O_3 (as spun)	4.20	1.69	2.48
PHB-CTS/3%Al_2O_3 (at day 100 degradation)	13.10	2.54	5.15

The absorption indexes (AI) calculated for spectroscopy of PHB-CTS/3%Al_2O_3 as spun and at day 100 of degradation, the results obtained here are tabulated in Table 8.

There exist many observations on the crystallinity increase in polymers through FTIR or DSC after degradation interval [117–120]. This phenomenon can be explained by the fact that the PBS molecules

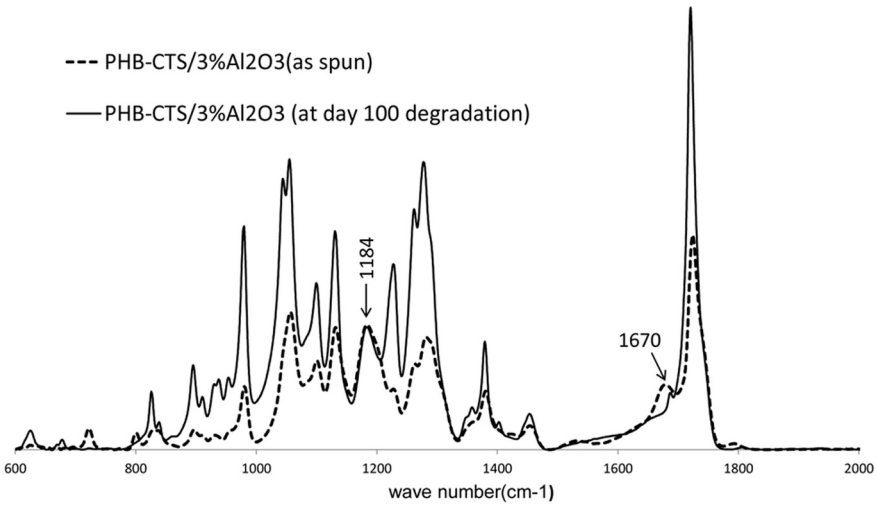

Fig. 12. The FTIR-ATR spectrum of PHB-CTS/3% Al_2O_3 composite scaffolds as spun and its degradation on 100 day.

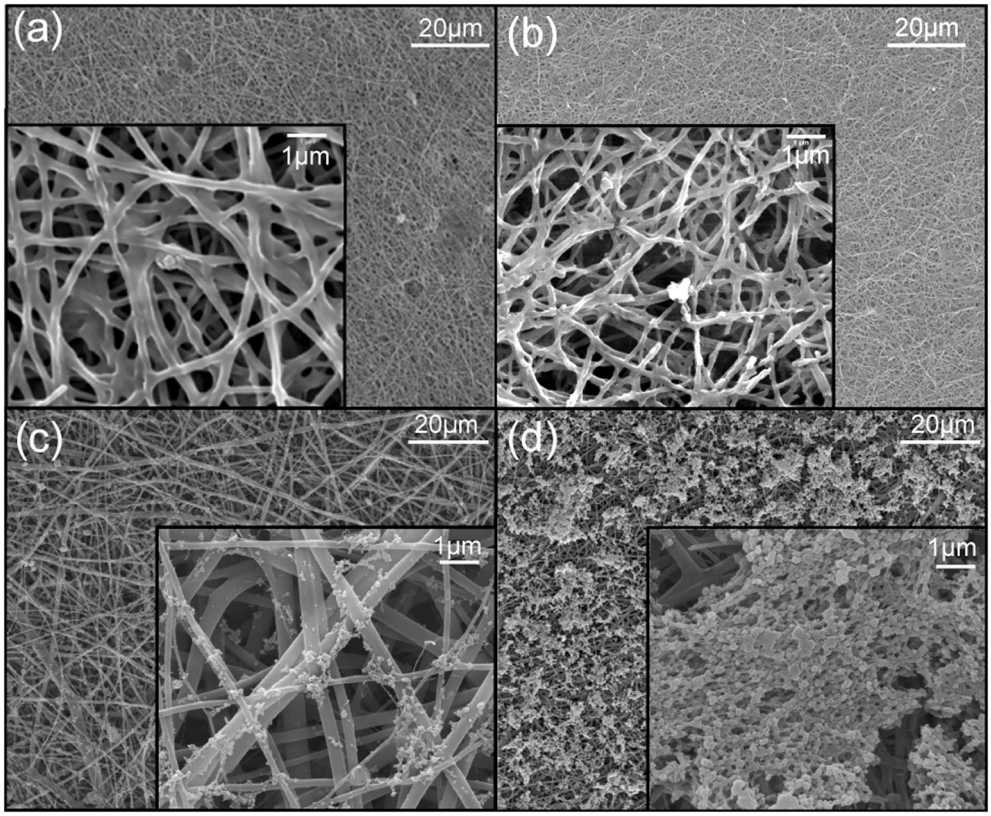

Fig. 13. SEM images of (a) PHB and (b) PHB-CTS at day 28 and PHB-CTS/3%Al_2O_3 composite scaffolds at (c) day 7 and (d) day 28, immersed in SBF.

diffuse easier in amorphous chain by breaking the amorphous chains. This rapid hydraulic degradation and the amorphous peaks thereof have less intensity after degradation. Breaking the chains in these areas reduce molecular entanglement degree and promote macromolecular chain mobility. Accordingly, this mobility leads to more ordered and re-aligned polymer chains and an increase in the crystallinity after degradation [118].

3.7. Assessment of bioactivity properties

3.7.1. Morphology of the fibers

One of the important aspect as to bone tissue engineering is the ability of bone bonding (bioactivity) [5,15]. The ability to form a hydroxyapatite (HA)-like surface layer is considered as one of the bioactivity indicators when the scaffold is immersed in SBF. The potential for formation of this layer through ion exchange phenomenon depends on substrate reactivity (dissolution–precipitation) [121]. This layer provides a physico-chemical and mechanical cohesion between the scaffold and the host bone during the biomineralization process [15].

The SEM images of PHB, PHB-CTS and PHB-CTS/3% Al_2O_3 composite scaffolds at day 28 immersion in SBF are shown in Fig. 13. For more accurate details, the scaffold containing Alumina nanowires is assessed on the 7th day as well. There is no considerable sediment on the surface of PHB as observed in Fig. 13(a). Although the effect of polysaccharides like CTS on bioactivity is reported by [15], in PHB-CTS the presence of sediment is hardly observed (Fig. 13(b)). The intriguing point in Fig. 13(c), is that some sediment is observed the PHB-CTS/3% Al_2O_3 composite scaffold at day 7, which is followed by complete coverage at day 28 as observed in Fig. 13(d). Increasing the hydrophilicity in the scaffolds can be a reason for the increase in sediment(s) accumulation [122]. Teimouri et al. reported an increase in biomineralization after adding γ-Alumina nanoparticles to silk fibroin/chitosan electrospun fibers [87].

3.7.2. Energy-dispersive X-ray spectroscopy (EDS)

To determine the chemical characteristics of these sediments, Energy-dispersive X-ray spectroscopy (EDS) is applied on Alumina contained scaffolds at days (a) 7 and (b) 28 immersed in SBF. Presence of calcium and phosphor in these sediments verified through EDS in Fig. 14. Although the results of EDS are not able to accurately determine the elements, presence of calcium and phosphorus in the sediment composite is confirmed.

3.7.3. X-ray diffraction analysis

To analysis and determine the structure of sediments, the X-ray diffraction is applied on PHB-CTS/3%Al_2O_3 composite scaffold at day 28 of immersion in SBF. There exist studies where that the peaks of PHB fibers appear at 2θ values of 13.2°, 17.1°, 25°, 26.5°, 26.7°, 28.5° and 31.6° assigned to (020), (110), (200), (021), (101), (121) and (002) of the orthorhombic unit cell, respectively [3,21,123]. Although the crystalline structure of PHB remains in during electrospinning process [21], presence of CTS, due to its amorphous nature, cause a decrease in its peak intensity. This *masking effect* due to intermolecular interactions, is already revealed by adding gelatin [116] and acetate cellulose [21] in the blend fibers based on PHB.

As observed in Fig. 15, formation of Calcium Phosphate ($Ca_2P_6O_{17}$) on the Alumina nanowires containing scaffolds surface is verified through XRD. The Calcium Phosphate peaks ($Ca_2P_6O_{17}$; JCPDS number: 00-43-0224) are appear at 2θ values of 17.19°, 19.33°, 22.21°, 24.9° and 26.8° assigned from (110), (−121), (−131), (002), (022) faces, confirm Calcium Phosphate deposition.

3.7.4. Cell viability assay

The MTT assay is run to assess the MG-63cell viability of PHB, PHB-CTS and PHB-CTS/3% Al_2O_3 composite scaffolds at days 1, 3, and 7. The maximum of MG-63 cell viability is for PHB-CTS/3% Al_2O_3 composite scaffolds and the minimum is for PHB are shown in Fig. 16. Low hydrophilicity of PHB is one of the most important factors in this

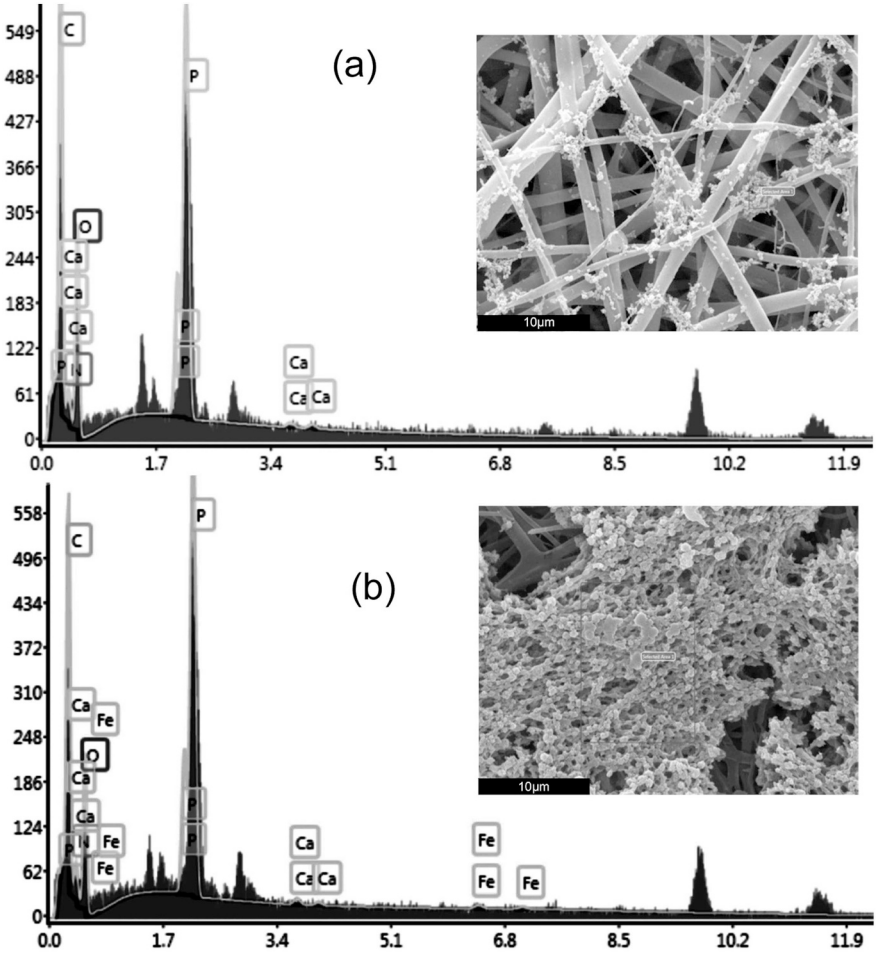

Fig. 14. Energy-dispersive X-ray spectroscopy of PHB-CTS/3%Al_2O_3 at days (a) 7 and (b) 28 immersed in SBF.

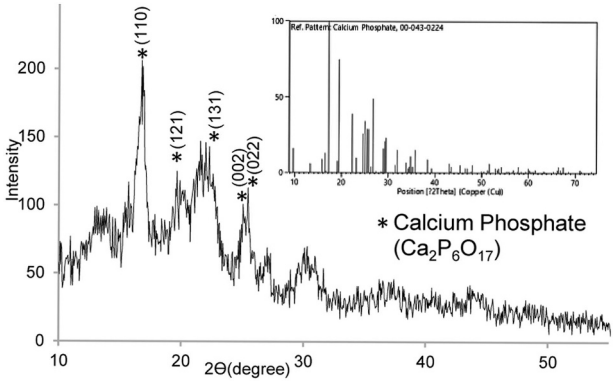

Fig. 15. XRD pattern of PHB-CTS/3% Al_2O_3 composite scaffold at day 28 immersed in SBF. The Insert image shows the standard pattern for calcium phosphate (00-043-0224).

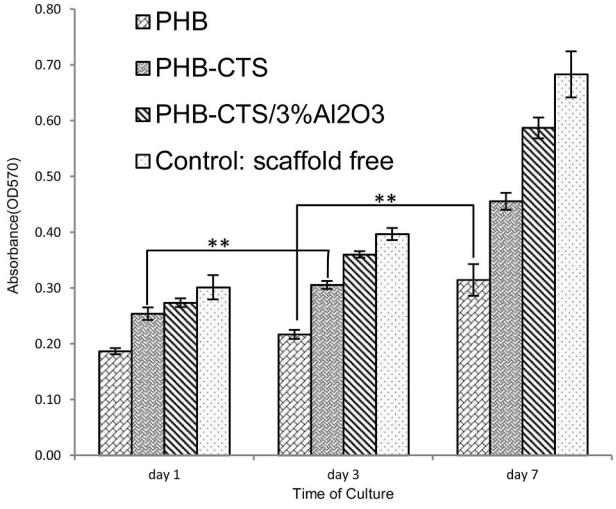

Fig. 16. Cell viability as indicated by MTT assay of MG-63 cells seeded on electrospun PHB, PHB-CTS and PHB-CTS/3%Al_2O_3nanowires at days 1, 3, and 7. (Statistical difference with $*p < 0.05$, $**p < 0.01$).

phenomenon. After adding CTS and Alumina which increase hydrophilicity, the absorption of essential proteins for cell to surface receptors' (vitronectin and fibronectin) binding increases and leads to enhanced cellular adhesion and proliferation [15,116,124].

3.7.5. Cell morphology studies

To assess the adhesion and proliferation of MG-63 cells, SEM images are shown in Fig. 17, at days 1 and 7 after the cell is cultured on PHB, PHB-CTS and PHB-CTS/3%Al_2O_3 composite scaffolds. The cells on pure PHB fibers are still in round-in shaped as observed in Fig. 17 (a, b), due to low hydrophilicity of PHB [19,21]. As observed for PHB-CTS (Fig. 17(c,d)) or PHB-CTS/3%Alumina composite scaffolds (Fig. 17(e,f)) cells adhere and are completely spread on the surface. They form a layer on the surface and have many pseudopodia. According to the obtained results, the growth and proliferation of MG-63 cells are higher in PHB-CTS/3%Al_2O_3 composite scaffolds than that of

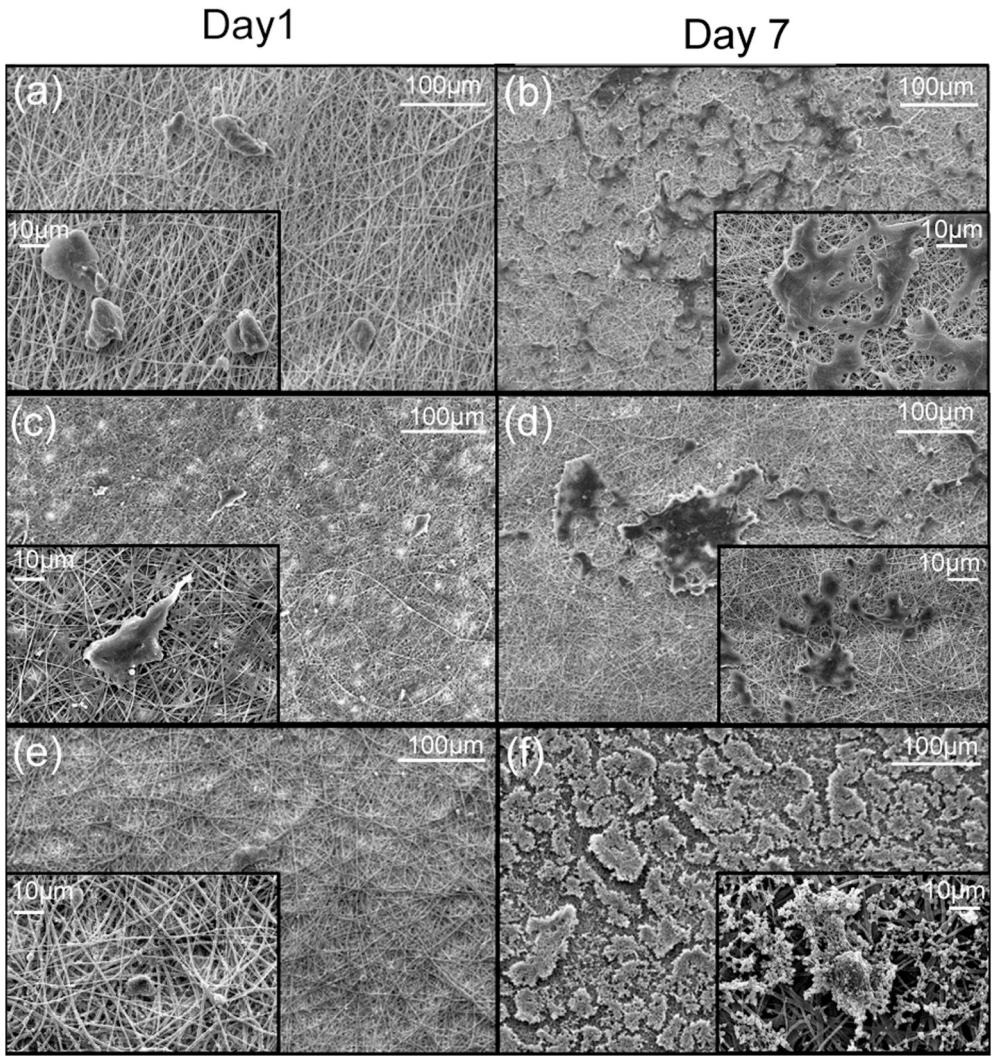

Fig. 17. SEM images of MG-63 cells seeded on electrospun scaffolds (a,b)PHB, (c,d)PHB-CTS and (e,f)PHB-CTS/3%Al_2O_3nanowires, right column at day1, left column at day 7.

the PHB or PHB-CTS. One reason, for this cell growth is the high hydrophilicity of the fiber, another reason is the increase in surface roughness of the fibers. The positive effects of increasing surface roughness on the adhesion of the MG-63 cell are studied by [54,125]. The presence of white calcium phosphate sediment layer is significant and is observed only in the scaffold containing Alumina at day 7, and even at day 1. The PCL fibers reinforced with Al_2O_3 whiskers, support fibroblast cell attachment and growth [35]. These findings demonstrate that adding Alumina nanowires will have positive affect on biological properties and compatibility of MG-63 cell attachment and growth, which being promising scaffolds for bone tissue engineering.

3.7.6. Alkaline phosphatase activity assay

Because a high amount of calcium phosphate which deposited on PHB-CTS/3% Al_2O_3 composite scaffolds even on the first week, in addition to the proper results from MTT and SEM for MG-63cell line, the alkaline phosphatase (ALP) secretion rate is assessed to estimate the activity of the osteoblasts. This activity of cultured MG-63 cells on PHB, PHB-CTS and PHB-CTS/3%Al_2O_3 composite scaffolds at weeks 1, 2 and 3 is shown in Fig. 18. It is observed that the alkaline phosphatase secretion on PHB-CTS is more than that of the PHB pure scaffolds, though not significant, ($p < 0.05$). The positive effect of CTS on ALP is studied by Jafary et al. [126]. The ALP secretion in the PHB-CTS/3%Al_2O_3 composite scaffolds is higher than other samples ($p < 0.05$), at during

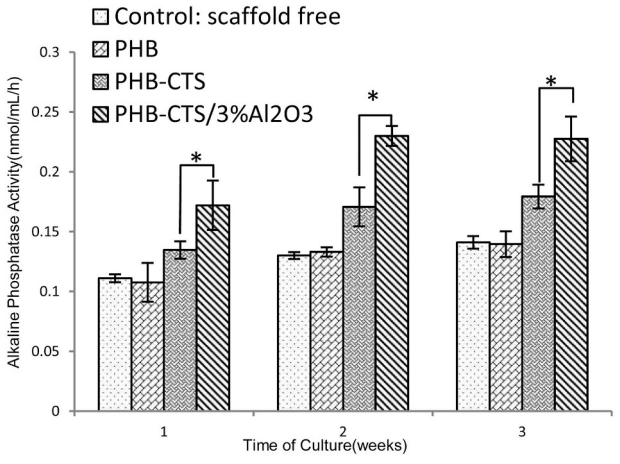

Fig. 18. ALP secretion of PHB, PHB-CTS and PHB-CTS/3%Al_2O_3 scaffolds at weeks 1, 2 and 3, (Statistical difference with $*p < 0.05$).

the culture. Webster et al. reported that synthesis of ALP and calcium-containing mineral sediment in nanophase Alumina [58]. Higher roughness on the surface of the fibers, and an increase in human mesenchymal stromal cells (hMSCs) adhesion, could also increase alkaline

phosphatase activity [4]. More roughness on the fibers can be another affecting factor. Although the osteointegration property (the ability to bonding with bone) of Titania is well known, some researchers reveal that both the Alumina and Titania in nanophase structure can increase osteoblast cells adhesion and alkaline phosphatase [54,58].

4. Conclusion

In this study, the PHB, PHB-CTS, PHB-CTS/3% Al_2O_3 nanowires composite scaffolds are prepared through the electrospinning method. The SEM results indicate an increase in fiber diameter due to presence of Alumina nanowires. TEM assessment reveals Alumina nanowires are aligned in the fibers. The distribution of nanowires in the composite scaffold is completely uniform according to Map of EDS studies. The FESEM indicate that presence of Alumina in the PHB-CTS alloy polymer increases wrinkle level on the surface of the fibers, thus, the causation of an increase surface roughness, confirmed by AFM. FTIR confirms the presence of Alumina in the scaffold, revealing a qualitative increase in crystallinity after adding Alumina nanowires to PHB-CTS scaffolds. This increase is confirmed by DSC studies. Scaffolds become more hydrophilic after Alumina is added. According to the mechanical properties, the tensile strength increases > 10 fold in presence of 3% wt Alumina. Presence of Alumina in the scaffolds increases the degradability (% weight loss) of pure PHB scaffold, although its degradation is less than that of the PHB-CTS scaffold. Degradation on amorphous and crystalline segments of the fibers can be easily observed by SEM. The FTIR results indicate an increase in crystallinity after degradation. This study indicates that calcium phosphate is deposited on Alumina containing scaffold after 7 and 28 days of immersion in SBF. Presence of this layer is confirmed by XRD. The EDS studies verify the existence of calcium and phosphate in the sediment. *In vitro* cell culture indicates that Alumina containing scaffold is appropriate in bone tissue engineering. Cell viability on scaffolds measured by microplate reader through MTT assay indicates a significantly higher value of absorption when MG-63 cells are cultured on Alumina contained scaffolds. The alkaline phosphatase secretion in the PHB-CTS/3%Al_2O_3 composite scaffolds is higher than other samples. The results indicate that PHB-CTS/3%Al_2O_3 nanocomposite can be an appropriate scaffold for bone tissue engineering applications.

Acknowledgments

This research was supported by Isfahan University of Medical Sciences (Iran) under grant number 395767. The Authors wish to thank Dr. Ali Zarrabi (Department of Biotechnology, Faculty of Advanced Sciences and Technologies, University of Isfahan, Isfahan) for his guidance in DSC discussions.

References

[1] S. Beck, T. Jiang, L. Nair, C. Laurencin, Chitosan for bone and cartilage regenerative engineering, Chitosan Based Biomaterials, Vol. 2 Elsevier, 2017, pp. 33–72.
[2] L. Roseti, V. Parisi, M. Petretta, C. Cavallo, G. Desando, I. Bartolotti, B. Grigolo, Scaffolds for bone tissue engineering: state of the art and new perspectives, Mater. Sci. Eng. C 78 (2017) 1246–1262.
[3] C. Zhijiang, Z. Cong, G. Jie, Z. Qing, Z. Kongyin, Electrospun carboxyl multi-walled carbon nanotubes grafted polyhydroxybutyrate composite nanofibers membrane scaffolds: preparation, characterization and cytocompatibility, Mater. Sci. Eng. C 82 (2018) 29–40.
[4] H. Chen, X. Huang, M. Zhang, F. Damanik, M.B. Baker, A. Leferink, H. Yuan, R. Truckenmüller, C. van Blitterswijk, L. Moroni, Tailoring surface nanoroughness of electrospun scaffolds for skeletal tissue engineering, Acta Biomater. 59 (2017) 82–93.
[5] S. Mallick, S. Tripathi, P. Srivastava, Advancement in scaffolds for bone tissue engineering: a review, IOSR J. Pharm. Biol. Sci 10 (2015) 37–54.
[6] D. Li, Y. Xia, Electrospinning of nanofibers: reinventing the wheel? Adv. Mater. 16 (14) (2004) 1151–1170.
[7] G. Wang, D. Yu, A.D. Kelkar, L. Zhang, Electrospun nanofiber: emerging reinforcing filler in polymer matrix composite materials, Prog. Polym. Sci. 75 (2017) 73–107.
[8] M. Sattary, M.T. Khorasani, M. Rafienia, H.S. Rozve, Incorporation of nanohydroxyapatite and vitamin D3 into electrospun PCL/gelatin scaffolds: the influence on the physical and chemical properties and cell behavior for bone tissue engineering, Polym. Adv. Technol. 29 (1) (2018) 451–462.
[9] S.K. Misra, S.N. Nazhat, S.P. Valappil, M. Moshrefi-Torbati, R.J. Wood, I. Roy, A.R. Boccaccini, Fabrication and characterization of biodegradable poly (3-hydroxybutyrate) composite containing bioglass, Biomacromolecules 8 (7) (2007) 2112–2119.
[10] B.D. Ratner, A.S. Hoffman, F.J. Schoen, J.E. Lemons, Biomaterials Science: An Introduction to Materials in Medicine, Elsevier, 2004.
[11] S.S.E. Bakhtiyari, S. Karbasi, A. Monshi, M. Montazeri, Evaluation of the effects of nano-TiO_2 on bioactivity and mechanical properties of nano bioglass-P3HB composite scaffold for bone tissue engineering, J. Mater. Sci. Mater. Med. 27 (1) (2016) 2.
[12] H. Hajiali, M. Hosseinalipour, S. Karbasi, M.A. Shokrgozar, The influence of bioglass nanoparticles on the biodegradation and biocompatibility of poly (3-hydroxybutyrate) scaffolds, Int. J. Artif. Organs 35 (11) (2012) 1015–1024.
[13] M. Zarei, S. Karbasi, Evaluation of the effects of multiwalled carbon nanotubes on electrospun poly (3-hydroxybutirate) scaffold for tissue engineering applications, J. Porous. Mater. 25 (1) (2018) 259–272.
[14] N. Thadavirul, P. Pavasant, P. Supaphol, Fabrication and evaluation of polycaprolactone–poly (hydroxybutyrate) or poly (3-hydroxybutyrate-co-3-hydroxyvalerate) dual-leached porous scaffolds for bone tissue engineering applications, Macromol. Mater. Eng. 302 (3) (2017).
[15] N. Goonoo, A. Bhaw-Luximon, P. Passanha, S.R. Esteves, D. Jhurry, Third generation poly (hydroxyacid) composite scaffolds for tissue engineering, J. Biomed. Mater. Res. B Appl. Biomater. 105 (6) (2017) 1667–1684.
[16] K. Rezwan, Q. Chen, J. Blaker, A.R. Boccaccini, Biodegradable and bioactive porous polymer/inorganic composite scaffolds for bone tissue engineering, Biomaterials 27 (18) (2006) 3413–3431.
[17] G.-Q. Chen, Q. Wu, The application of polyhydroxyalkanoates as tissue engineering materials, Biomaterials 26 (33) (2005) 6565–6578.
[18] S. Köse, F.A. Kaya, E.B. Denkbaş, P. korkusuz, F.D. cetinkaya, Evaluation of biocompatibility of random or aligned electrospun polyhydroxybutyrate scaffolds combined with human mesenchymal stem cells, Turk. J. Biol. 40 (2) (2016) 410–419.
[19] D. Sadeghi, S. Karbasi, S. Razavi, S. Mohammadi, M.A. Shokrgozar, S. Bonakdar, Electrospun poly (hydroxybutyrate)/chitosan blend fibrous scaffolds for cartilage tissue engineering, J. Appl. Polym. Sci. 133 (47) (2016).
[20] G. Ramanathan, S. Singaravelu, M. Raja, N. Nagiah, P. Padmapriya, K. Ruban, K. Kaveri, T. Natarajan, U.T. Sivagnanam, P.T. Perumal, Fabrication and characterization of a collagen coated electrospun poly (3-hydroxybutyric acid)–gelatin nanofibrous scaffold as a soft bio-mimetic material for skin tissue engineering applications, RSC Adv. 6 (10) (2016) 7914–7922.
[21] C. Zhijiang, X. Yi, Y. Haizheng, J. Jia, Y. Liu, Poly (hydroxybutyrate)/cellulose acetate blend nanofiber scaffolds: preparation, characterization and cytocompatibility, Mater. Sci. Eng. C 58 (2016) 757–767.
[22] R. LogithKumar, A. KeshavNarayan, S. Dhivya, A. Chawla, S. Saravanan, N. Selvamurugan, A review of chitosan and its derivatives in bone tissue engineering, Carbohydr. Polym. 151 (2016) 172–188.
[23] S. Deepthi, J. Venkatesan, S.-K. Kim, J.D. Bumgardner, R. Jayakumar, An overview of chitin or chitosan/nano ceramic composite scaffolds for bone tissue engineering, Int. J. Biol. Macromol. 93 (2016) 1338–1353.
[24] S.K.L. Levengood, M. Zhang, Chitosan-based scaffolds for bone tissue engineering, J. Mater. Chem. B 2 (21) (2014) 3161–3184.
[25] S. Saravanan, R. Leena, N. Selvamurugan, Chitosan based biocomposite scaffolds for bone tissue engineering, Int. J. Biol. Macromol. 93 (2016) 1354–1365.
[26] F. Croisier, C. Jérôme, Chitosan-based biomaterials for tissue engineering, Eur. Polym. J. 49 (4) (2013) 780–792.
[27] S. Karbasi, Z.M. Alizadeh, Effects of multi-wall carbon nanotubes on structural and mechanical properties of poly (3-hydroxybutyrate)/chitosan electrospun scaffolds for cartilage tissue engineering, Bull. Mater. Sci. 40 (6) (2017) 1247–1253.
[28] M.R. Foroughi, S. Karbasi, M. Khoroushi, A.A. Khademi, Polyhydroxybutyrate/chitosan/bioglass nanocomposite as a novel electrospun scaffold: fabrication and characterization, J. Porous. Mater. 24 (6) (2017) 1447–1460.
[29] K.I. Winey, R.A. Vaia, Polymer nanocomposites, MRS Bull. 32 (4) (2007) 314–322.
[30] J. Ji, G. Sui, Y. Yu, Y. Liu, Y. Lin, Z. Du, S. Ryu, X. Yang, Significant improvement of mechanical properties observed in highly aligned carbon-nanotube-reinforced nanofibers, J. Phys. Chem. C 113 (12) (2009) 4779–4785.
[31] R. Sen, B. Zhao, D. Perea, M.E. Itkis, H. Hu, J. Love, E. Bekyarova, R.C. Haddon, Preparation of single-walled carbon nanotube reinforced polystyrene and polyurethane nanofibers and membranes by electrospinning, Nano Lett. 4 (3) (2004) 459–464.
[32] J. Lee, Y. Deng, Increased mechanical properties of aligned and isotropic electrospun PVA nanofiber webs by cellulose nanowhisker reinforcement, Macromol. Res. 20 (1) (2012) 76–83.
[33] O.J. Rojas, G.A. Montero, Y. Habibi, Electrospun nanocomposites from polystyrene loaded with cellulose nanowhiskers, J. Appl. Polym. Sci. 113 (2) (2009) 927–935.
[34] J. Sapkota, A. Shirole, E.J. Foster, J.C.M. Garcia, M. Lattuada, C. Weder, Polymer nanocomposites with nanorods having different length distributions, Polymer 110 (2017) 284–291.
[35] Z. Dong, Y. Wu, Q. Wang, C. Xie, Y. Ren, R.L. Clark, Reinforcement of electrospun membranes using nanoscale Al_2O_3 whiskers for improved tissue scaffolds, J. Biomed. Mater. Res. A 100 (4) (2012) 903–910.
[36] S.-Y. Fu, B. Lauke, The elastic modulus of misaligned short-fiber-reinforced

polymers, Compos. Sci. Technol. 58 (3–4) (1998) 389–400.
[37] D. Gupta, J. Venugopal, S. Mitra, V.G. Dev, S. Ramakrishna, Nanostructured biocomposite substrates by electrospinning and electrospraying for the mineralization of osteoblasts, Biomaterials 30 (11) (2009) 2085–2094.
[38] N. Bleach, S. Nazhat, K. Tanner, M. Kellomäki, P. Törmälä, Effect of filler content on mechanical and dynamic mechanical properties of particulate biphasic calcium phosphate—polylactide composites, Biomaterials 23 (7) (2002) 1579–1585.
[39] W. Murphy, J. Black, G.W. Hastings, Handbook of Biomaterial Properties, Springer, 2016.
[40] J.E. Tercero, S. Namin, D. Lahiri, K. Balani, N. Tsoukias, A. Agarwal, Effect of carbon nanotube and aluminum oxide addition on plasma-sprayed hydroxyapatite coating's mechanical properties and biocompatibility, Mater. Sci. Eng. C 29 (7) (2009) 2195–2202.
[41] E. Garcia-Cimbrelo, Alumina-on-alumina in total hip arthroplasty: a five-to 15-year follow-up study, Bone Joint J. 98 (SUPP 1) (2016) 149.
[42] M. Shahid, D. Shikha, S. Sinha, U. Jha, S. Murugesan, E. Mohandas, D. Kothari, Morphological Study of HAP Coated Alumina by Sol-Gel Method for Orthopedic Implants, Advanced Materials Research, Trans Tech Publ, (2015), pp. 50–60.
[43] G.-C. Lee, R.H. Kim, Incidence of modern alumina ceramic and alumina matrix composite femoral head failures in nearly 6 million hip implants, J. Arthroplast. 32 (2) (2017) 546–551.
[44] M. Zhao, Y. Sun, J. Zhang, Y. Zhang, Novel translucent and strong submicron alumina ceramics for dental restorations, J. Dent. Res. 0022034517733742 (2017).
[45] J. Fan, T. Lin, F. Hu, Y. Yu, M. Ibrahim, R. Zheng, S. Huang, J. Ma, Effect of sintering temperature on microstructure and mechanical properties of zirconia-toughened alumina machinable dental ceramics, Ceram. Int. 43 (4) (2017) 3647–3653.
[46] C.F. Caravaca, Q. Flamant, M. Anglada, L. Gremillard, J. Chevalier, Impact of sandblasting on the mechanical properties and aging resistance of alumina and zirconia based ceramics, J. Eur. Ceram. Soc. 38 (3) (2018) 915–925.
[47] S.S. Bristy, M.A. Rahman, K. Tauer, H. Minami, H. Ahmad, Preparation and characterization of magnetic γ-Al_2O_3 ceramic nanocomposite particles with variable Fe_3O_4 content and modification with epoxide functional polymer, Ceram. Int. 44 (2017) 3951–3959.
[48] J.F. DeWilde, H. Chiang, D.A. Hickman, C.R. Ho, A. Bhan, Kinetics and mechanism of ethanol dehydration on γ-Al_2O_3: the critical role of dimer inhibition, ACS Catal. 3 (4) (2013) 798–807.
[49] S. Vivekchand, U. Ramamurty, C. Rao, Mechanical properties of inorganic nanowire reinforced polymer–matrix composites, Nanotechnology 17 (11) (2006) S344.
[50] A. Gupta, G. Tripathi, D. Lahiri, K. Balani, Compression molded ultra high molecular weight polyethylene–hydroxyapatite–aluminum oxide–carbon nanotube hybrid composites for hard tissue replacement, J. Mater. Sci. Technol. 29 (6) (2013) 514–522.
[51] F.A. Alzarrug, M.M. Dimitrijević, R.M.J. Heinemann, V. Radojević, D.B. Stojanović, P.S. Uskoković, R. Aleksić, The use of different alumina fillers for improvement of the mechanical properties of hybrid PMMA composites, Mater. Des. 86 (2015) 575–581.
[52] L. Rodríguez-Lorenzo, A. Salinas, M. Vallet-Regí, J. San Roman, Composite biomaterials based on ceramic polymers. I. Reinforced systems based on Al2O3/PMMA/PLLA, J. Biomed. Mater. Res. A 30 (4) (1996) 515–522.
[53] M. Hashimoto, J.I. Sasaki, S. Imazato, Investigation of the cytotoxicity of aluminum oxide nanoparticles and nanowires and their localization in L 929 fibroblasts and RAW 264 macrophages, J. Biomed. Mater. Res. B Appl. Biomater. 104 (2) (2016) 241–252.
[54] T.J. Webster, R.W. Siegel, R. Bizios, Osteoblast adhesion on nanophase ceramics, Biomaterials 20 (13) (1999) 1221–1227.
[55] Y. Song, Y. Ju, G. Song, Y. Morita, In vitro proliferation and osteogenic differentiation of mesenchymal stem cells on nanoporous alumina, Int. J. Nanomedicine 8 (2013) 2745.
[56] M. Karlsson, E. Pålsgård, P.R. Wilshaw, L. Di Silvio, Initial in vitro interaction of osteoblasts with nano-porous alumina, Biomaterials 24 (18) (2003) 3039–3046.
[57] Y. Song, Y. Ju, Y. Morita, B. Xu, G. Song, Surface functionalization of nanoporous alumina with bone morphogenetic protein 2 for inducing osteogenic differentiation of mesenchymal stem cells, Mater. Sci. Eng. C 37 (2014) 120–126.
[58] T.J. Webster, C. Ergun, R.H. Doremus, R.W. Siegel, R. Bizios, Enhanced functions of osteoblasts on nanophase ceramics, Biomaterials 21 (17) (2000) 1803–1810.
[59] J. Ramier, T. Bouderlique, O. Stoilova, N. Manolova, I. Rashkov, V. Langlois, E. Renard, P. Albanese, D. Grande, Biocomposite scaffolds based on electrospun poly (3-hydroxybutyrate) nanofibers and electrosprayed hydroxyapatite nanoparticles for bone tissue engineering applications, Mater. Sci. Eng. C 38 (2014) 161–169.
[60] Y. Liu, M. Wang, Thermophysical and mechanical properties of β-tricalcium phosphate reinforced polyhydroxybutyrate and polyhydroxybutyrate-co-hydroxyvalerate composites, Key Engineering Materials, Trans Tech Publ, 2007, pp. 1217–1220.
[61] D. Kai, H.M. Chong, L.P. Chow, L. Jiang, Q. Lin, K. Zhang, H. Zhang, Z. Zhang, X.J. Loh, Strong and biocompatible lignin/poly (3-hydroxybutyrate) composite nanofibers, Compos. Sci. Technol. 158 (2018) 26–33.
[62] A.L. Yarin, S. Koombhongse, D.H. Reneker, Bending instability in electrospinning of nanofibers, J. Appl. Phys. 89 (5) (2001) 3018–3026.
[63] Y. Ji, K. Liang, X. Shen, G.L. Bowlin, Electrospinning and characterization of chitin nanofibril/polycaprolactone nanocomposite fiber mats, Carbohydr. Polym. 101 (2014) 68–74.
[64] S. Karbasi, M. Zarei, M. Foroughi, Effects of multi-wall carbon nano-tubes (MWNTs) on structural and mechanical properties of electrospun poly (3-hydroxybutyrate) scaffold for tissue engineering applications, Sci. Iran 23 (6) (2016) 3145.
[65] Y. Liu, S. Wang, R. Zhang, Composite poly (lactic acid)/chitosan nanofibrous scaffolds for cardiac tissue engineering, Int. J. Biol. Macromol. 103 (2017) 1130–1137.
[66] P. Wutticharoenmongkol, N. Sanchavanakit, P. Pavasant, P. Supaphol, Preparation and characterization of novel bone scaffolds based on electrospun polycaprolactone fibers filled with nanoparticles, Macromol. Biosci. 6 (1) (2006) 70–77.
[67] L. Moroni, R. Licht, J. de Boer, J.R. de Wijn, C.A. van Blitterswijk, Fiber diameter and texture of electrospun PEOT/PBT scaffolds influence human mesenchymal stem cell proliferation and morphology, and the release of incorporated compounds, Biomaterials 27 (28) (2006) 4911–4922.
[68] L. Ghasemi-Mobarakeh, D. Semnani, M. Morshed, A novel method for porosity measurement of various surface layers of nanofibers mat using image analysis for tissue engineering applications, J. Appl. Polym. Sci. 106 (4) (2007) 2536–2542.
[69] A.S. Asran, Electrospinning of Polymeric Nanofibers and Nanocomposite Materials: Fabrication, Physicochemical Characterization and Medical Applications, Martin-Luther-Universität Halle-Wittenberg, 2011, p. 152.
[70] N.J. Hallab, K.J. Bundy, K. O'Connor, R.L. Moses, J.J. Jacobs, Evaluation of metallic and polymeric biomaterial surface energy and surface roughness characteristics for directed cell adhesion, Tissue Eng. 7 (1) (2001) 55–71.
[71] R. Price, K. Haberstroh, T. Webster, Enhanced functions of osteoblasts on nanostructured surfaces of carbon and alumina, Med. Biol. Eng. Comput. 41 (3) (2003) 372–375.
[72] B.D. Boyan, T.W. Hummert, D.D. Dean, Z. Schwartz, Role of material surfaces in regulating bone and cartilage cell response, Biomaterials 17 (2) (1996) 137–146.
[73] Z. Wang, M. Song, C. Sun, Y. He, Effects of particle size and distribution on the mechanical properties of SiC reinforced Al–Cu alloy composites, Mater. Sci. Eng. A 528 (3) (2011) 1131–1137.
[74] M.P. Reddy, F. Ubaid, R. Shakoor, G. Parande, V. Manakari, A. Mohamed, M. Gupta, Effect of reinforcement concentration on the properties of hot extruded Al-Al_2O_3 composites synthesized through microwave sintering process, Mater. Sci. Eng. A 696 (2017) 60–69.
[75] J. Chen, Q. Yu, G. Zhang, S. Yang, J. Wu, Q. Zhang, Preparation and biocompatibility of nanohybrid scaffolds by in situ homogeneous formation of nano hydroxyapatite from biopolymer polyelectrolyte complex for bone repair applications, Colloids Surf. B: Biointerfaces 93 (2012) 100–107.
[76] D. Ciprari, K. Jacob, R. Tannenbaum, Characterization of polymer nanocomposite interphase and its impact on mechanical properties, Macromolecules 39 (19) (2006) 6565–6573.
[77] A.C. Mottin, E. Ayres, R.L. Oréfice, J.J.D. Câmara, What changes in poly (3-hydroxybutyrate)(PHB) when processed as electrospun nanofibers or thermo-compression molded film? Mater. Res. 19 (1) (2016) 57–66.
[78] Q.P. Pham, U. Sharma, A.G. Mikos, Electrospinning of polymeric nanofibers for tissue engineering applications: a review, Tissue Eng. 12 (5) (2006) 1197–1211.
[79] A.S. Asran, K. Razghandi, N. Aggarwal, G.H. Michler, T. Groth, Nanofibers from blends of polyvinyl alcohol and polyhydroxy butyrate as potential scaffold material for tissue engineering of skin, Biomacromolecules 11 (12) (2010) 3413–3421.
[80] A. Romo-Uribe, A. Meneses-Acosta, M. Domínguez-Díaz, Viability of HEK 293 cells on poly-β-hydroxybutyrate (PHB) biosynthesized from a mutant *Azotobacter vinelandii* strain. Cast film and electrospun scaffolds, Mater. Sci. Eng. C 81 (2017) 236–246.
[81] M.P. Arrieta, J. López, D. López, J. Kenny, L. Peponi, Development of flexible materials based on plasticized electrospun PLA–PHB blends: structural, thermal, mechanical and disintegration properties, Eur. Polym. J. 73 (2015) 433–446.
[82] T. Furukawa, H. Sato, R. Murakami, J. Zhang, Y.-X. Duan, I. Noda, S. Ochiai, Y. Ozaki, Structure, dispersibility, and crystallinity of poly (hydroxybutyrate)/poly (L-lactic acid) blends studied by FT-IR microspectroscopy and differential scanning calorimetry, Macromolecules 38 (15) (2005) 6445–6454.
[83] N. Naveen, R. Kumar, S. Balaji, T. Uma, T. Natrajan, P. Sehgal, Synthesis of nonwoven nanofibers by electrospinning–a promising biomaterial for tissue engineering and drug delivery, Adv. Eng. Mater. 12 (8) (2010).
[84] L.S. Guinesi, É.T.G. Cavalheiro, Influence of some reactional parameters on the substitution degree of biopolymeric Schiff bases prepared from chitosan and salicylaldehyde, Carbohydr. Polym. 65 (4) (2006) 557–561.
[85] O. Urbanek, P. Sajkiewicz, F. Pierini, The effect of polarity in the electrospinning process on PCL/chitosan nanofibres' structure, properties and efficiency of surface modification, Polymer 124 (2017) 168–175.
[86] L. Medvecky, M. Giretova, R. Stulajterova, Properties and in vitro characterization of polyhydroxybutyrate–chitosan scaffolds prepared by modified precipitation method, J. Mater. Sci. Mater. Med. 25 (3) (2014) 777–789.
[87] A. Teimouri, R. Ebrahimi, A.N. Chermahini, R. Emadi, Fabrication and characterization of silk fibroin/chitosan/nano γ-alumina composite scaffolds for tissue engineering applications, RSC Adv. 5 (35) (2015) 27558–27570.
[88] A.K. Patel, K. Balani, Dispersion fraction enhances cellular growth of carbon nanotube and aluminum oxide reinforced ultrahigh molecular weight polyethylene biocomposites, Mater. Sci. Eng. C 46 (2015) 504–513.
[89] A.K. Patel, P. Trivedi, K. Balani, Processing and mechanical characterization of compression-molded ultrahigh molecular weight polyethylene biocomposite reinforced with aluminum oxide, J. Nanosci. Nanoeng. Appl. 4 (3) (2014) 1–11.
[90] T.A. Saleh, V.K. Gupta, Synthesis and characterization of alumina nano-particles polyamide membrane with enhanced flux rejection performance, Sep. Purif. Technol. 89 (2012) 245–251.
[91] M. Vallet-Regí, S. Granado, D. Arcos, M. Gordo, M. Cabanas, C. Ragel, A. Salinas,

A. Doadrio, J. San Román, Preparation, characterization, and in vitro release of ibuprofen from Al2O3/PLA/PMMA composites, J. Biomed. Mater. Res. 39 (3) (1998) 423–428.
[92] L. Rodríguez-Lorenzo, A. Salinas, M. Vallet-Regí, J. San Roman, Composite biomaterials based on ceramic polymers. I. Reinforced systems based on Al2O3/PMMA/PLLA, J. Biomed. Mater. Res. 30 (4) (1996) 515–522.
[93] M. Porter, J. Yu, Crystallization kinetics of poly (3-hydroxybutyrate) granules in different environmental conditions, J. Biomed. Nanotechnol. 2 (03) (2011) 301.
[94] J. Xu, B.-H. Guo, R. Yang, Q. Wu, G.-Q. Chen, Z.-M. Zhang, In situ FTIR study on melting and crystallization of polyhydroxyalkanoates, Polymer 43 (25) (2002) 6893–6899.
[95] C. Wang, C.-H. Hsu, I.-H. Hwang, Scaling laws and internal structure for characterizing electrospun poly [(R)-3-hydroxybutyrate] fibers, Polymer 49 (19) (2008) 4188–4195.
[96] M.K. Cheung, K.P. Wan, P.H. Yu, Miscibility and morphology of chiral semicrystalline poly-(R)-(3-hydroxybutyrate)/chitosan and poly-(R)-(3-hydroxybutyrate-co-3-hydroxyvalerate)/chitosan blends studied with DSC, 1H T1 and T1ρ CRAMPS, J. Appl. Polym. Sci. 86 (5) (2002) 1253–1258.
[97] T. Ikejima, Y. Inoue, Crystallization behavior and environmental biodegradability of the blend films of poly (3-hydroxybutyric acid) with chitin and chitosan, Carbohydr. Polym. 41 (4) (2000) 351–356.
[98] T. Ikejima, K. Yagi, Y. Inoue, Thermal properties and crystallization behavior of poly (3-hydroxybutyric acid) in blends with chitin and chitosan, Macromol. Chem. Phys. 200 (2) (1999) 413–421.
[99] S. Nandagopal, R. Augustine, S.C. George, V. Jayachandran, N. Kalarikkal, S. Thomas, Gentamicin loaded electrospun poly (ε-caprolactone)/TiO_2 nanocomposite membranes with antibacterial property against methicillin resistant *Staphylococcus aureus*, Polym.-Plast. Technol. Eng. 55 (2016) 1785.
[100] A.M. Díez-Pascual, A.L. Díez-Vicente, ZnO-reinforced poly (3-hydroxybutyrate-co-3-hydroxyvalerate) bionanocomposites with antimicrobial function for food packaging, ACS Appl. Mater. Interfaces 6 (12) (2014) 9822–9834.
[101] S.Y.H. Abdalkarim, H.-Y. Yu, D. Wang, J. Yao, Electrospun poly (3-hydroxybutyrate-co-3-hydroxy-valerate)/cellulose reinforced nanofibrous membranes with ZnO nanocrystals for antibacterial wound dressings, Cellulose 24 (7) (2017) 2925–2938.
[102] H. Lee, K. Yamaguchi, T. Nagaishi, M. Murai, M. Kim, K. Wei, K.-Q. Zhang, I.S. Kim, Enhancement of mechanical properties of polymeric nanofibers by controlling crystallization behavior using a simple freezing/thawing process, RSC Adv. 7 (69) (2017) 43994–44000.
[103] E. Kuzelova Kostakova, L. Meszaros, G. Maskova, L. Blazkova, T. Turcsan, D. Lukas, Crystallinity of electrospun and centrifugal spun polycaprolactone fibers: a comparative study, J. Nanomater. 2017 (2017).
[104] G. Ma, D. Yang, K. Wang, J. Han, S. Ding, G. Song, J. Nie, Organic-soluble chitosan/polyhydroxybutyrate ultrafine fibers as skin regeneration prepared by electrospinning, J. Appl. Polym. Sci. 118 (6) (2010) 3619–3624.
[105] H. Rodríguez-Tobías, G. Morales, A. Ledezma, J. Romero, R. Saldívar, V. Langlois, E. Renard, D. Grande, Electrospinning and electrospraying techniques for designing novel antibacterial poly (3-hydroxybutyrate)/zinc oxide nanofibrous composites, J. Mater. Sci. 51 (18) (2016) 8593–8609.
[106] M.P. Arrieta, J. López, D. López, J.M. Kenny, L. Peponi, Effect of chitosan and catechin addition on the structural, thermal, mechanical and disintegration properties of plasticized electrospun PLA-PHB biocomposites, Polym. Degrad. Stab. 132 (2016) 145–156.
[107] R. Rajan, P. Sreekumar, K. Joseph, M. Skrifvars, Thermal and mechanical properties of chitosan reinforced polyhydroxybutyrate composites, J. Appl. Polym. Sci. 124 (4) (2012) 3357–3362.
[108] S.Y. Chan, B.Q.Y. Chan, Z. Liu, B.H. Parikh, K. Zhang, Q. Lin, X. Su, D. Kai, W.S. Choo, D.J. Young, Electrospun pectin-polyhydroxybutyrate nanofibers for retinal tissue engineering, ACS Omega 2 (12) (2017) 8959–8968.
[109] F. Lamastra, A. Bianco, A. Meriggi, G. Montesperelli, F. Nanni, G. Gusmano, Nanohybrid PVA/ZrO_2 and PVA/Al_2O_3 electrospun mats, Chem. Eng. J. 145 (1) (2008) 169–175.
[110] A. Arinstein, M. Burman, O. Gendelman, E. Zussman, Effect of supramolecular structure on polymer nanofibre elasticity, Nat. Nanotechnol. 2 (1) (2007) 59.
[111] S.-C. Wong, A. Baji, S. Leng, Effect of fiber diameter on tensile properties of electrospun poly (ε-caprolactone), Polymer 49 (21) (2008) 4713–4722.
[112] J.H. Park, G.C. Rutledge, Ultrafine high performance polyethylene fibers, J. Mater. Sci. 53 (4) (2018) 3049–3063.
[113] Y. Dong, S. Liao, M. Ngiam, C.K. Chan, S. Ramakrishna, Degradation behaviors of electrospun resorbable polyester nanofibers, Tissue Eng. B Rev. 15 (3) (2009) 333–351.
[114] M. Zhang, N.L. Thomas, Blending polylactic acid with polyhydroxybutyrate: the effect on thermal, mechanical, and biodegradation properties, Adv. Polym. Technol. 30 (2) (2011) 67–79.
[115] S.-G. Hong, Y.-C. Lin, C.-H. Lin, Crystallization and degradation behaviors of treated polyhydroxybutyrates, React. Funct. Polym. 68 (11) (2008) 1516–1523.
[116] N. Nagiah, L. Madhavi, R. Anitha, N.T. Srinivasan, U.T. Sivagnanam, Electrospinning of poly (3-hydroxybutyric acid) and gelatin blended thin films: fabrication, characterization, and application in skin regeneration, Polym. Bull. 70 (8) (2013) 2337–2358.
[117] Y. Marois, Z. Zhang, M. Vert, X. Deng, R. Lenz, R. Guidoin, Mechanism and rate of degradation of polyhydroxyoctanoate films in aqueous media: a long-term in vitro study, J. Biomed. Mater. Res. A 49 (2) (2000) 216–224.
[118] A.W. Shum, A.F. Mak, Morphological and biomechanical characterization of poly (glycolic acid) scaffolds after in vitro degradation, Polym. Degrad. Stab. 81 (1) (2003) 141–149.
[119] J. Ferreira, A. Gloria, S. Cometa, J.F. Coelho, M. Domingos, Effect of in vitro enzymatic degradation on 3d printed poly (ε-caprolactone) scaffolds: morphological, chemical and mechanical properties, J. Appl. Biomater. Funct. Mater. 15 (3) (2017) 185–195.
[120] V. Zhuikov, A. Bonartsev, D. Bagrov, S. Yakovlev, V. Myshkina, T. Makhina, I. Bessonov, M. Kopitsyna, A. Morozov, A. Rusakov, Mechanics and surface ultrastructure changes of poly (3-hydroxybutyrate) films during enzymatic degradation in pancreatic lipase solution, Mol. Cryst. Liq. Cryst. 648 (1) (2017) 236–243.
[121] M. Neo, T. Nakamura, T. Yamamuro, C. Ohtsuki, T. Kokubo, Bone Bonding Biomaterials, by P. Ducheyne, T. Kokubo and CA van Blitterswijk, Reed Healthcare Communications, Leiderdrop, The Netherlands, 1993, pp. 111–121.
[122] R. Balu, S. Singaravelu, N. Nagiah, Bioceramic nanofibres by electrospinning, Fibers 2 (3) (2014) 221–239.
[123] H.E. Salama, G.R. Saad, M.W. Sabaa, Synthesis, characterization and antimicrobial activity of biguanidinylated chitosan-g-poly [(R)-3-hydroxybutyrate], Int. J. Biol. Macromol. 101 (2017) 438–447.
[124] X. Yang, K. Zhao, G.-Q. Chen, Effect of surface treatment on the biocompatibility of microbial polyhydroxyalkanoates, Biomaterials 23 (5) (2002) 1391–1397.
[125] R.L. Price, M.C. Waid, K.M. Haberstroh, T.J. Webster, Selective bone cell adhesion on formulations containing carbon nanofibers, Biomaterials 24 (11) (2003) 1877–1887.
[126] F. Jafary, J. Varshosaz, M. Panjehpour, P. Yaghmaei, Immobilization of alkaline phosphatase using chitosan nanoparticles, Russ. J. Appl. Chem. 88 (5) (2015) 891–897.